Title: Comparative analysis of BCG vaccination routes in mice reveals preferential reprogramming of pulmonary macrophages upon mucosal administration.

Authors: Aaron James Forde[1,8]*, Mara Esposito[1]*, Emanuela Kerschbamer[1]*, David Schreiner[1], Eduardo Moreo[1], Nikos Pantouloufos[1], Jean de Lima[1], Habiba Soliman[1], Maike Erber[1], Claire E. Depew[1], Wadschma Naderi[1] and Carolyn G. King[1,8].

[1]: Infection Immunology Laboratory, Department of Biomedicine, University of Basel, Basel, CH 4058, Switzerland.

[8]: Lead contacts.

***These authors contributed equally.**

Corresponding authors:

Aaron J. Forde and Carolyn G. King

Department of Biomedicine

University of Basel

Mattenstrasse 28

CH-4058 Basel, Switzerland

Email: aaronjames.forde@unibas.ch; carolyn.king@unibas.ch

Tel: +41 61 207 5080 (AJF); +41 78 907 15 68 (CGK)

Abstract:

Bacille Calmette-Guérin (BCG) is the only licensed vaccine against tuberculosis (TB) but provides inconsistent protection against disease. Studies in non-human primates show that intravenous BCG confers superior protection compared to intradermal vaccination, yet how different vaccination routes reprogram lung immunity in mice - the primary model for mechanistic studies - remains incompletely defined at single cell or spatial resolution. Lung resident macrophages, including alveolar macrophages (AM) and interstitial macrophages (IM), are key effector cells during *Mycobacterium tuberculosis* infection, but most studies have focused on AM, leaving IM responses to vaccination largely unexplored. Here, we define the cellular and spatial immune landscape shaped by three BCG vaccination routes in mice using flow cytometry, single-cell RNA sequencing, and spatial transcriptomics. Comparing intratracheal (IT), intravenous (IV), and subcutaneous (SC) vaccination, we demonstrate that mucosal IT delivery uniquely reprograms interstitial macrophages, establishes spatially organized immune hubs with CD4 T cells, and provides superior protection against infectious challenge. These findings identify IM as key mediators of mucosal vaccine-induced protection and provide a framework for the rational optimization of vaccines against respiratory pathogens.

Introduction

Tuberculosis (TB) remains one of the world's deadliest infectious diseases, causing an estimated 10.8 million cases and 1.25 million deaths in 2023, with the highest burden in resource limited low- and middle-income countries (1). Despite widespread use for over a century, Bacillus Calmette-Guérin (BCG) remains the only licensed vaccine against TB and provides inconsistent protection against pulmonary disease. A deeper understanding of the immune mechanisms underlying durable protection is urgently needed.

Lung macrophages are among the first immune cells to encounter *Mycobacterium tuberculosis* (Mtb), the causative agent of TB, following inhalation. Two major macrophage subsets inhabit the lung: alveolar macrophages (AM), which reside in the airspaces, and interstitial macrophages (IM), which occupy the lung parenchyma (2). These macrophages differ in origin, metabolic state and antimicrobial capacity. AM are the earliest responders to Mtb, and accumulating evidence suggests that prior vaccination can metabolically and epigenetically reprogram them to restrict Mtb growth, ultimately reducing early bacterial burden and shaping the trajectory of disease progression (3,4). In comparison, the precise nature of IM rewiring following BCG vaccination is less well understood. Surface marker expression levels of CD206, CD11c, MHCII, Lyve1, CX3CR1 and CD169 have been used by different groups in an effort to further describe IM heterogeneity in the naive lung (5–7). Additional work to better characterize different subgroups of IM has shown a distinct functional separation based on expressed chemokines (8). However, how IM might be modulated during infection remains largely unknown. Upon niche depletion, Ly6c-high monocytes undergo local proliferation in an M-CSF and MafB dependent manner before differentiating into IM (9). This process was shown to additionally depend on TGFβ signaling (10). Moreover, evidence suggests that the role of IM during pulmonary infection may be context dependent. For example, IM have been shown to be permissive to *Klebsiella pneumoniae* and depletion of IM in a fungal infection model resulted in significantly reduced pathogen load (11,12). In contrast, mouse models of Mtb infection have shown that IM are more restrictive to bacterial growth as compared to AM (13,14).

Although BCG is typically administered intradermally, recent studies demonstrate that vaccination route significantly impacts protective immunity against Mtb. In non-human primates, IV BCG

78 vaccination induced markedly higher frequencies of antigen-responsive CD4 and CD8 T cells in
79 blood, lung parenchyma, and bronchoalveolar lavage fluid compared to intradermal vaccination,
80 and conferred robust protection following Mtb challenge (15,16). Subsequent studies showed that
81 high-dose IV BCG drives an influx of polyfunctional T cells and recruited macrophages into
82 airways, with both CD4+ and CD8α+ T cells required for protection (15,17). Similar route
83 dependent effects have been observed in mice. Intranasal but not subcutaneous BCG vaccination
84 activates AM, enhancing metabolic and activation gene signatures and improving bacterial control
85 after both Mtb and *Streptococcus pneumoniae* challenge (18). More recently, IV BCG was shown
86 to generate a CX3CR1-high CD4+ effector memory T cell subset capable of mediating cross
87 protection against influenza via IFNγ dependent activation of AM (19).
88
89 Collectively, these findings suggest that vaccination route shapes immune responses in the lung,
90 with protection strongly correlating with enhanced T cell and macrophage activation. However,
91 studies to date have focused primarily on AM while the impact on IM biology remains largely
92 unexplored. Notably, IM express high levels of the anti-microbial effector NOS2 during Mtb
93 infection in mice suggesting a potential role in early bacterial control (14). Whether vaccination,
94 particularly via alternative routes, enhances IM antimicrobial capacity remains unknown. This gap
95 is especially relevant given growing interest in mucosal vaccination strategies which may directly
96 engage pulmonary macrophages at the site of pathogen entry and negate safety concerns associated
97 with IV BCG injection.
98
99 To directly compare how vaccine delivery route shapes lung macrophage biology, we immunized
100 mice with BCG via SC, IV, or mucosal IT administration. High-dimensional flow cytometry and
101 single-cell RNA sequencing (scRNA-Seq) revealed that IT vaccination selectively expands a
102 distinct IM subset enriched for metabolic, antimicrobial, and type I/II IFN-response programs that
103 were not observed after SC or IV delivery. Consistent with these findings, IT BCG elicited the
104 strongest protection in Mtb rechallenge experiments. Integration of cell-cell interaction analyses
105 and spatial transcriptomics uncovered potential IM - CD4 T cell interactions and demonstrated
106 that activated IM localize to distinct regions of the lung following IT BCG. Together, these
107 findings identify IM reprogramming as a previously underappreciated component of mucosal BCG

108 immunity and highlight mucosal vaccination as a promising strategy to harness lung macrophages
109 for improved protection against Mtb.

110 **Results.**

111 **IT BCG supports enhanced IM activation.**

112 Given that lung macrophages are among the first immune cells to encounter pulmonary Mtb, we
113 focused on how the route of BCG vaccination differentially rewired these cells. Wild type (WT)
114 mice were vaccinated with SC, IT, or IV BCG, and after 8 weeks lungs were harvested and
115 analyzed by high dimensional flow cytometry using a gating strategy designed to identify AM, IM
116 as well as other myeloid cells (Supplementary Fig. 1 A).
117
118 The frequency of AM was reduced after IT and IV vaccination compared to naïve mice but the
119 absolute numbers remained unchanged (Fig. 1 A). Analysis of typical macrophage activation
120 markers including CD80, CD86 and MHCII revealed increased expression after IT and IV, but not
121 SC, vaccination in AM (Fig. 1 B). CD38 has recently been described as a marker of macrophages
122 which possess an enhanced ability to control Mtb (20). Following IT and IV vaccination the
123 frequency of CD38 positive AM was increased (Fig. 1 C). In contrast, SC BCG did not lead to
124 enhanced CD38 expression on AM (Fig. 1 C). The frequency of NOS2 positive AM increased by
125 a small but significant extent following IT and IV, but not SC, vaccination (Fig. 1 D). We next
126 examined the AM phenotype at an earlier time point of 4 weeks post vaccination. Following IT
127 and IV vaccination the expression of CD80, CD86 and MHCII was increased on AM, as was the
128 frequency of CD38 positive cells. Similar to the 8-week time point, SC BCG did not enhance the
129 expression of the analyzed markers (Supplementary Fig. 1 B-D). At a later timepoint of 12 weeks
130 post vaccination the increased expression of CD86 and MHCII was maintained in IT and IV
131 vaccinated groups as compared to naive or SC vaccinated mice (Supplementary Fig. 1 E).
132 Increased frequencies of CD38 or NOS2 positive AM were only observed in the IT vaccinated
133 group (Supplementary Fig. 1 F, G).
134
135 Within the IM compartment we observed an increase in both cell frequency and absolute numbers
136 8 weeks after IT BCG (Fig. 1 E). Analysis of activation markers revealed increased expression of
137 CD80, no change in CD86 and downregulation of MHCII after IT and IV BCG (Fig. 1 F). In
138 contrast to AM, the frequency of CD38 positive IM increased after all routes of vaccination (Fig.

139 1 G), while NOS2 expression was significantly increased only after IT BCG (Fig. 1 H), suggesting
140 route-specific enhancement of antimicrobial effector capacity. At 4 weeks post vaccination CD80
141 expression was increased after IT and IV BCG, however CD86 and MHCII levels were decreased
142 (Supplementary Fig. 1 H). Furthermore, IT and IV BCG also increased the frequencies of both
143 CD38 and NOS2 positive cells (Supplementary Fig. 1 I, J). By 12 weeks post vaccination IM from
144 IT BCG mice maintained elevated CD80 expression, whereas the expression of the other analyzed
145 markers appeared to be returning to baseline (Supplementary Fig. 1 K-M). Together, these data
146 indicate that IT and IV BCG exert significant alterations to the phenotype of both AM and IM,
147 while SC BCG has a minimal impact.
148
149 Since viable BCG is present up to 12 weeks post IT and IV vaccination (Supplementary Fig. 1 N),
150 we next wondered if the continued presence of bacteria was required for driving the expression of
151 CD80, CD86 and MHCII by AM or IM. To examine this, cohorts of WT mice were vaccinated
152 using SC, IT or IV routes for a period of 8 weeks. Next, the animals were administered a cocktail
153 of antibiotics (rifampicin and isoniazid) in the drinking water for 4 weeks. Following a rest period
154 of 2 weeks, the lungs were harvested and analyzed using flow cytometry. We observed similar
155 expression of CD80, CD86 and MHCII by AM after all routes of vaccination in antibiotic treated
156 and untreated mice (Supplementary Fig. 1 O). In the case of IM, antibiotic treatment did not
157 influence the expression of these markers, with the exception of increased MHCII expression in
158 IT-vaccinated mice (Supplementary Fig. 1 P).
159

Figure 1

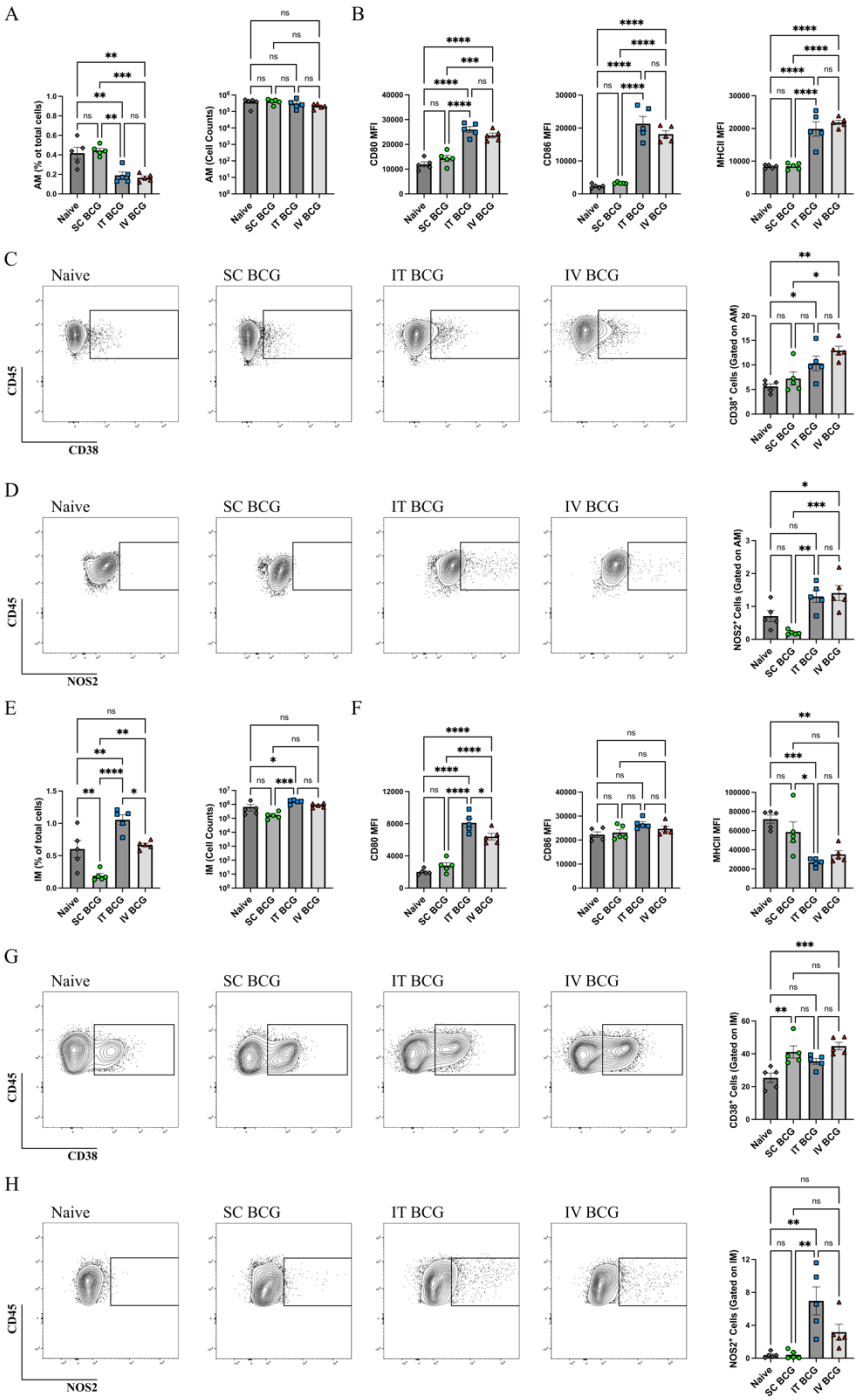

160

161

162

163 **Figure 1. IT BCG supports enhanced IM activation.**
164 **(A)**: Frequency of total lung cells and absolute numbers of AM 8 weeks after SC, IT and IV BCG
165 vaccination. **(B)**: Mean Fluorescence Intensity (MFI) of CD80, CD86 and MHCII expressed by
166 AM after BCG vaccination. **(C, D)**: Representative plots and quantification of CD38 or NOS2
167 positive AM 8 weeks after BCG vaccination. **(E)**: Frequency of total lung cells and absolute
168 numbers of IM 8 weeks after SC, IT and IV BCG vaccination. **(F)**: MFI of CD80, CD86 and
169 MHCII on IM 8 weeks vaccination. **(G, H)**: Representative plots and quantification of CD38 or
170 NOS2 positive IM 8 weeks after BCG vaccination. N: Each datapoint indicates one individual
171 mouse. One-Way ANOVA with Tukey's multiple comparison test was used to determine statistical
172 significance.
173
174
175 To more comprehensively characterize the transcriptional programs underlying changes in
176 macrophage phenotype, we next used scRNA-Seq to more thoroughly investigate these cells.
177 CD45 positive cells were sorted from the lungs of naive mice as well as those that had been
178 vaccinated with SC, IT or IV BCG 8 weeks prior. The cell suspensions were stained with CITE-
179 seq antibodies to facilitate the identification of the various immune cell populations. We began our
180 analysis by focusing on myeloid cells and using surface markers as well as known marker genes,
181 we identified AM, IM, DCs and monocytes (Fig. 2 A, Supplementary Fig. 2 A-D). It was notable
182 that among these populations SC BCG appeared to have a minimal impact on the transcriptome of
183 AM and IM (Supplementary Fig. 2 E). In contrast IT and IV BCG resulted in alterations to the
184 transcriptomic profile of both cell types (Supplementary Fig. 2 F, G).
185 Pseudobulk differential expression analysis further revealed that IV BCG led to the most
186 upregulated genes in AM as compared to naïve controls (Supplementary Fig. 2 H), while IT BCG-
187 treated AM showed increased expression of antigen presentation genes *(H2-K1*, *H2-Ab1*) as well
188 as the chaperone protein *Cd74* (Supplementary Fig. 2 J). We next focused our analysis on IM after
189 vaccination and observed that IT BCG had the most profound effect in terms of the number of
190 upregulated genes (Fig. 2 B). Within these upregulated genes were a number of interferon targets
191 such as *Cxcl9*, *Gbp2, Stat1* and *Cd274* (Fig. 2 C). In addition, IM from IT BCG vaccinated mice
192 expressed several metabolic genes including *Gapdh*, *Nampt*, *Pkm*, *Fth1, Slc2a1* as well as *Acod1*
193 (Fig. 2 C). In line with this, gene set enrichment analysis revealed increased activity in pathways

194 associated with IFNγ response, OXPHOS and glycolysis in IM from IT vaccinated mice (Fig. 2
195 D). Given that the aforementioned analysis was performed on all IM, we wondered if only a subset
196 of IM were responsible for driving the expression of these pathways. We identified 6 clusters of
197 IM in naïve and vaccinated mice of which cluster 1 was present only after IT and IV vaccination
198 (Fig. 2 E, F). In order to examine if the IM within cluster 1 were the cells primarily activated
199 following BCG vaccination, we created a gene expression signature score (named activated IM)
200 based on the genes upregulated after IT BCG. This signature score was most highly expressed by
201 the IM present in cluster 1 (Fig. 2 G) indicating that this subset was primarily activated after IT
202 BCG.
203
204
205
206

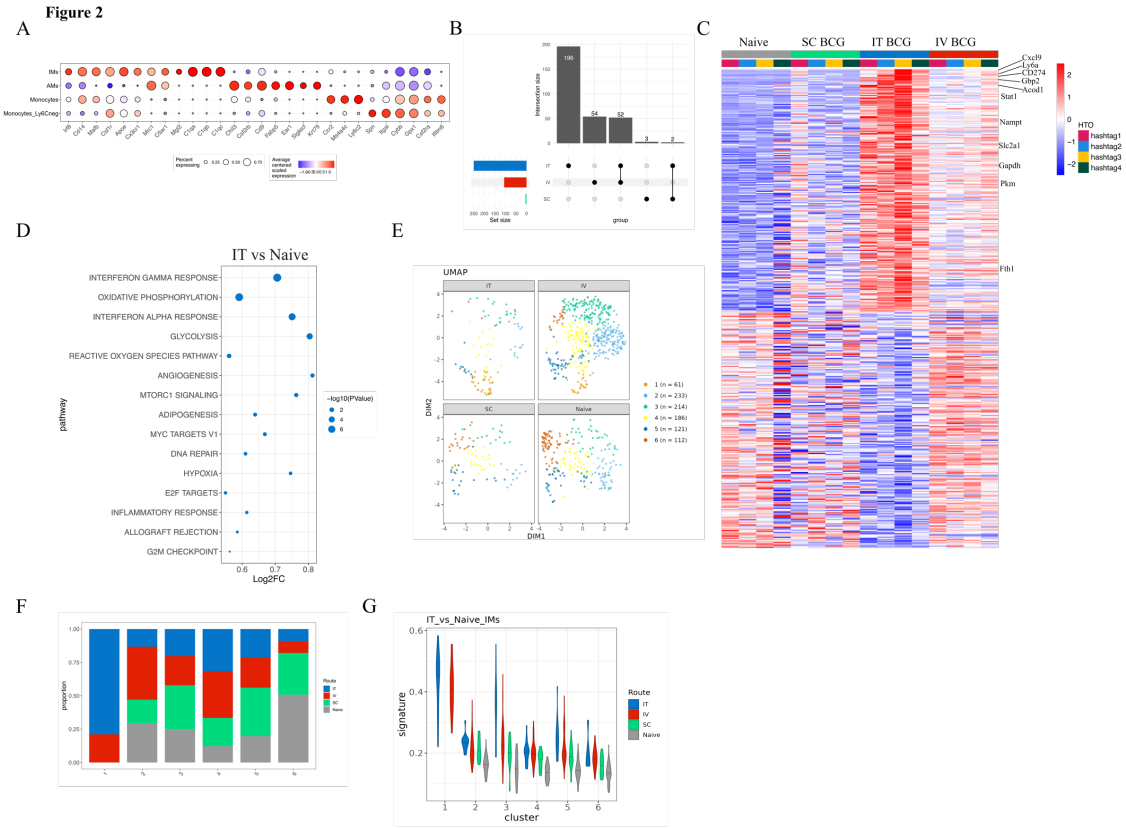

Figure 2. IT BCG transcriptionally rewires IM.

(A): Expression of signature genes used to identify AM, IM, Ly6C high and Ly6C low monocytes in the single cell RNA Seq dataset. **(B):** Upset plot depicting the number of genes upregulated by IM after each route of BCG vaccination as compared to naïve cells. **(C)**: Heatmap depicting genes upregulated by IM following IT BCG vaccination. **(D)**: Pathway enrichment analysis performed on the genes upregulated by IM 8 weeks after IT BCG vaccination. **(E):** UMAP displaying IM clusters that were present after SC, IT or IV BCG vaccination. **(F):** Proportion of IM clusters described in (E). **(G)**: Violin plot depicting the activated IM expression signature score in each IM cluster.

218

219 **CD4 T cells likely produce IFNγ after all routes of BCG vaccination.**

220 Given that IM from IT vaccinated mice showed enrichment for IFNγ-response genes (Fig. 2 C-D),
221 we next sought to identify which immune cells were producing IFNγ. To do this we examined the
222 non-myeloid immune cells within our single cell data set and based on marker genes and surface
223 protein expression identified B cells, NK cells, as well as CD4 and CD8 T cells (Supplementary
224 Fig. 3 A, B). Within these lymphocyte populations *Ifng* expression was highest in the CD4 T cell
225 compartment (Supplementary Fig. 3 C). We therefore focused on examining route dependent
226 differences in CD4 T cells following BCG vaccination. 5 clusters of CD4 T cells were identified
227 in naïve and BCG vaccinated mice (Supplementary Fig. 3 D). Cluster 5 was present predominantly
228 in unvaccinated mice and were likely unactivated cells. Clusters 2 and 4 expressed genes such as
229 *Sell*, *Ccr7* and *S1pr1,* these are expressed by naïve and central memory CD4 T cells
230 (Supplementary Fig. 3 E, F). Despite sharing the expression of the above-mentioned genes, clusters
231 2 and 4 differed in their distribution among the experimental groups. Specifically, cluster 2 was
232 present only after IT and IV BCG while cluster 4 was present in SC vaccinated mice
233 (Supplementary Fig. 3 G). Genes higher in cluster 2 than cluster 4 suggest more active translational
234 machinery: *Eif3f* (a component of the translation initiation complex), the transcription factor *Klf13*,
235 *Chd3* (involved in chromatin remodeling), *Tut4* (involved in mRNA decay) and *Pnrc1*
236 (Supplementary Fig. 3 E, F).

237

238 Cluster 1 was present in all conditions but at a higher proportion in IT and IV vaccinated mice
239 (Supplementary Fig. 3 G). This cluster resembled migrating CD4 T cells (*Maf* and *Cxcr3*) and a
240 small proportion of Tfh cells (*Bcl6*, *Pdcd1*, *Izumo1r*, *Cxcr5*) (21). We next performed pseudobulk
241 differential expression analysis and compared how the CD4 T cells within cluster 1 differed after
242 each route of vaccination. After IT and IV vaccination, cells in cluster 1 had a higher expression
243 of both *Socs1* and *Jund* as compared to SC BCG, potentially indicating a more regulatory
244 phenotype (Fig. 3 A, B). In addition, *Tgfb* expression was increased after IT and IV as compared
245 to SC BCG. Beyond its role in tissue remodeling, TGFβ signaling has recently been described to
246 mediate the transition of monocytes to IM in the lung (10) and is required for AM survival (2,22).
247 Interestingly, when comparing cells within cluster 1 in the IT and IV groups, we observed
248 increased expression of *Hk2* in the IT group which may be indicative of enhanced metabolic

activity. These cells also exhibited higher expression of *Cxcr4* (a Tfh marker) and *Cxcr6* (a Th1 marker), genes which are involved in the homing to, and retention in, inflamed tissue (Fig. 3 C).

CD4 T cells within cluster 3 expressed genes such as *Cx3cr1*, *Zeb2*, *Il18rap* and *Ifng* (Supplementary Fig. 3 E, F). This cluster resembled a recently described effector memory subset of CX3CR1^{Hi} CD4 T cells that are induced following IV BCG (19). To confirm this apparent similarity, we generated a gene expression signature score (named activated CD4 cells) based on the aforementioned publication and overlaid it onto our single cell dataset. As expected, cluster 3 had the highest signature expression score followed by cluster 1 (Fig. 3 E, F). Notably, cluster 3 CD4 T cells were present at similar proportions across all vaccination routes (Supplementary Fig. 3 G), prompting us to investigate whether functional differences might be more apparent at the transcriptional level. Pseudobulk differential expression demonstrated that cluster 3 CD4 T cells were broadly similar after IT and IV BCG but clustered separately in SC BCG mice (Supplementary Fig. 3 I). When comparing IT and SC routes we observed that the cells from the IT mice expressed metabolic genes such as *Glud1*, *Acadl*, *Coq2*, *Mff*, and *Tomm20* suggesting an enhanced oxidative metabolism typical of memory cells. Moreover, they expressed genes indicative of a regulatory profile like *Tgfb1, Ltb* and *Socs1* as well as the anti-apoptotic genes *Mcl1* and *Bag1* (Fig. 3. G). In contrast, CD4 T cells within cluster 3 from SC BCG mice appeared to be in a more inflammatory state. These cells expressed *Cd9* (a tetraspanin associated with immune synapse formation), *Cxcl10* (involved in T cell recruitment), *Csf1* (indicating ongoing communication with monocytes or macrophages) and *Tnfrsf4* (OX40, a costimulatory receptor) (Fig. 3 G). Similar gene expression patterns were observed when cluster 3 CD4 T cells were examined in the IV versus SC groups (Fig. 3 H). To complement these data, we performed additional flow cytometry experiments with a panel targeting CD4 T lymphocytes (Supplementary Fig. 3 J). 8 weeks after vaccination the absolute cell number of total CD4 T cells was increased in IT BCG mice (Supplementary Fig. 3 K, L). In addition, the frequency and number of tissue resident CD45 IV negative CD4 T cells was increased after IT BCG (Fig. 3 J-L). In line with this we observed an increase in the number of total CD4 T cells expressing the residency marker CD69 (Fig. 3 M). Further, CD45 IV negative CD4 T cells from IT BCG mice increased expression of CD44, CXCR3 and CXCR6, collectively indicating enhanced activation and potential tissue retention (Fig. 3 N-P).

Figure 3

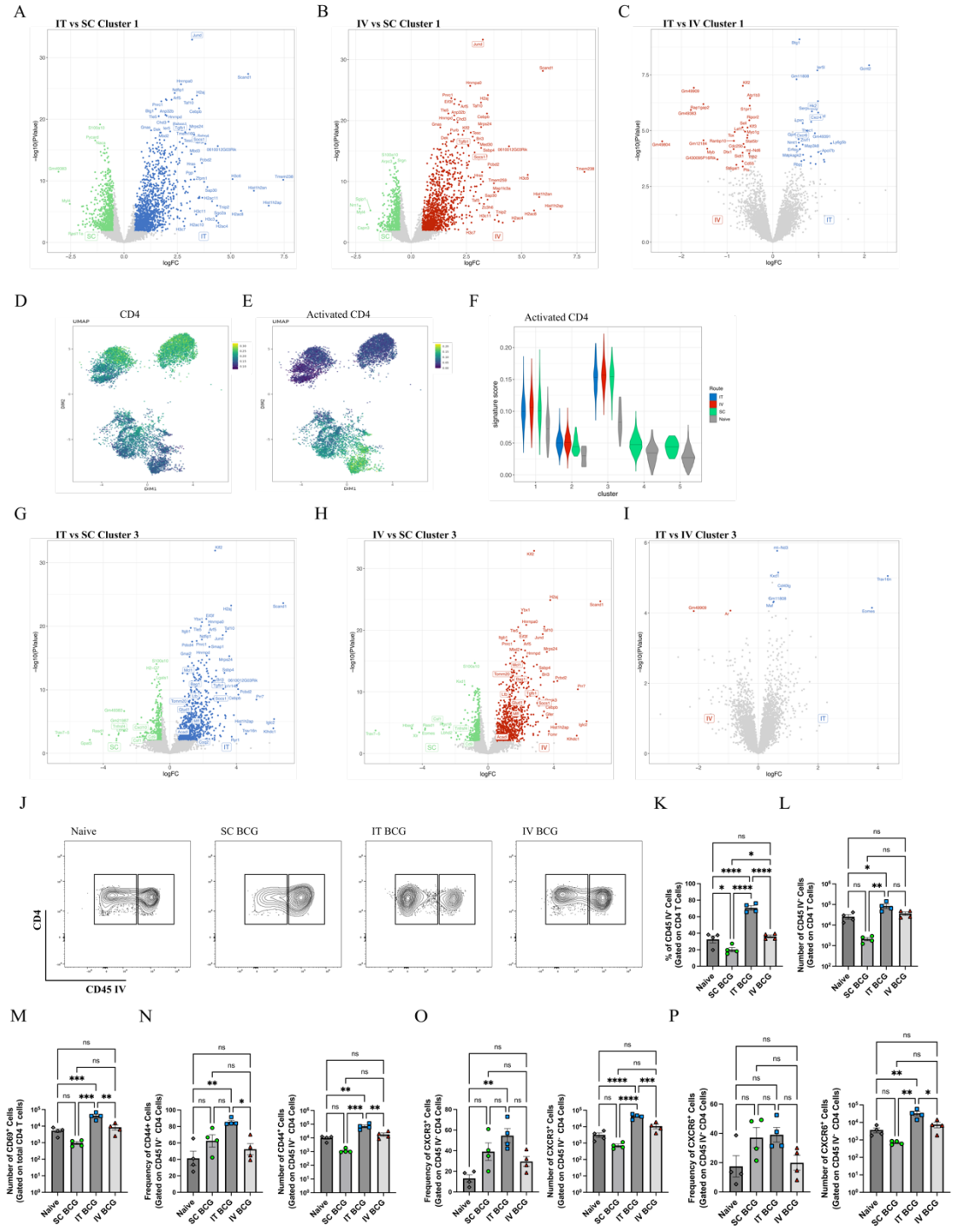
A
IT vs SC Cluster 1
B
IV vs SC Cluster 1
C
IT vs IV Cluster 1
D
CD4
E
Activated CD4
F
Activated CD4
signature score
cluster
Route
IT
IV
SC
Naive
G
IT vs SC Cluster 3
H
IV vs SC Cluster 3
I
IT vs IV Cluster 3
J
Naive
SC BCG
IT BCG
IV BCG
CD4
CD45 IV
K
% of CD45 IV⁺ Cells (Gated on CD4 T Cells)
L
Number of CD45 IV⁺ Cells (Gated on CD4 T Cells)
M
Number of CD69⁺ Cells (Gated on total CD4 T cells)
N
Frequency of CD44⁺ Cells (Gated on CD45 IV⁻ CD4 Cells)
Number of CD44⁺ Cells (Gated on CD45 IV⁻ CD4 Cells)
O
Frequency of CXCR3⁺ Cells (Gated on CD45 IV⁻ CD4 Cells)
Number of CXCR3⁺ Cells (Gated on CD45 IV⁻ CD4 Cells)
P
Frequency of CXCR6⁺ Cells (Gated on CD45 IV⁻ CD4 Cells)
Number of CXCR6⁺ Cells (Gated on CD45 IV⁻ CD4 Cells)
Naive
SC BCG
IT BCG
IV BCG

283

284 **Figure 3. CD4 T cells likely produce IFNγ after all routes of BCG vaccination.**

285 **(A-C)**: Volcano plots depicting DEGs in cluster 1 CD4 T cells IT vs SC (A), IV vs SC (B) or IT
286 vs IV (C). (**D-E**) Expression of the CD4 and activated CD4 signature score on the clusters of CD4
287 T cells. **(F)**: Violin plot depicting the strength of the activated CD4 expression signature in each
288 CD4 T cell cluster. **(G-I)**: Volcano plots depicting DEGs in cluster 3 CD4 T cells IT vs SC (G),
289 IV vs SC (H) or IT vs IV (I). **(J)**: Representative plots depicting the proportions of CD45 IV
290 positive and negative CD4 T cells in naive mice or in animals vaccinated with SC, IT or IV BCG
291 8 weeks prior. **(K, L)**: Frequency (K) and absolute number (L) of CD45 negative CD4 T cells in
292 naive and vaccinated mice. **(M)**: Number of CD69 positive, resident CD4 T cells in naive mice
293 and those vaccinated 8 weeks prior. **(N-P)**: Frequency and absolute numbers of CD45 negative
294 CD4 T cells expressing CD44 (N), CXCR3 (O) and CXCR6 (P). For Fig. 3 K-P, N: Each datapoint
295 indicates one individual mouse. One-Way ANOVA with Tukey's multiple comparison test was
296 used to determine statistical significance.

297

298 **IM-CD4 T cell crosstalk following BCG Vaccination.**

299 Having identified route specific differences in both IM and CD4 T cell phenotypes, we next
300 performed NicheNet analysis to understand if these cell types were directly interacting. For this
301 analysis we separated CD4 T cells from cluster 3 (labeled activated CD4 T cells) from the other
302 clusters (labeled as CD4 T cells). This confirmed that activated CD4 T cells were the primary
303 potential source of IFNγ for IM after all vaccination routes (Fig. 4 A-C) and that this was signaling
304 via *Ifngr1* and *Ifngr2* on IM (Supplementary Fig. 4 A-C). Next, we wondered if IM were
305 reciprocally signaling to CD4 T cells. NicheNet analysis predicted that after IT BCG, IM signal to
306 CD4 T cells primarily via the chemokines *Ccl3*, *Cxcl10* and *Cxcl16* (Fig. 4 E). *Cxcl16* was
307 predicted to signal via *Cxcr6* (Supplementary Fig. 4 E). The predicted *Cxcl16*/*Cxcr6* signaling axis
308 was consistent with our flow cytometry data showing increased CXCR6 expression on CD4 T cells
309 after IT vaccination (Fig. 3 N-P). IM from IV BCG mice were similarly providing *Ccl3* and *Cxcl16*
310 (Fig. 4 F). In contrast to IT and IV vaccination, CD4 T cells from SC BCG mice were not receiving
311 these ligands from IM and instead were receiving a distinct set of signals including *Il-1b,* as well
312 as *Ifng* from activated CD4 T cells (Fig. 4 D). Collectively these data suggest that mucosal IT
313 vaccination establishes a bidirectional IM-CD4 T cell circuit such that IM derived CXCL16

promotes the recruitment of CD4 T cells to the lung, which in turn provide IFNγ to sustain IM activation.

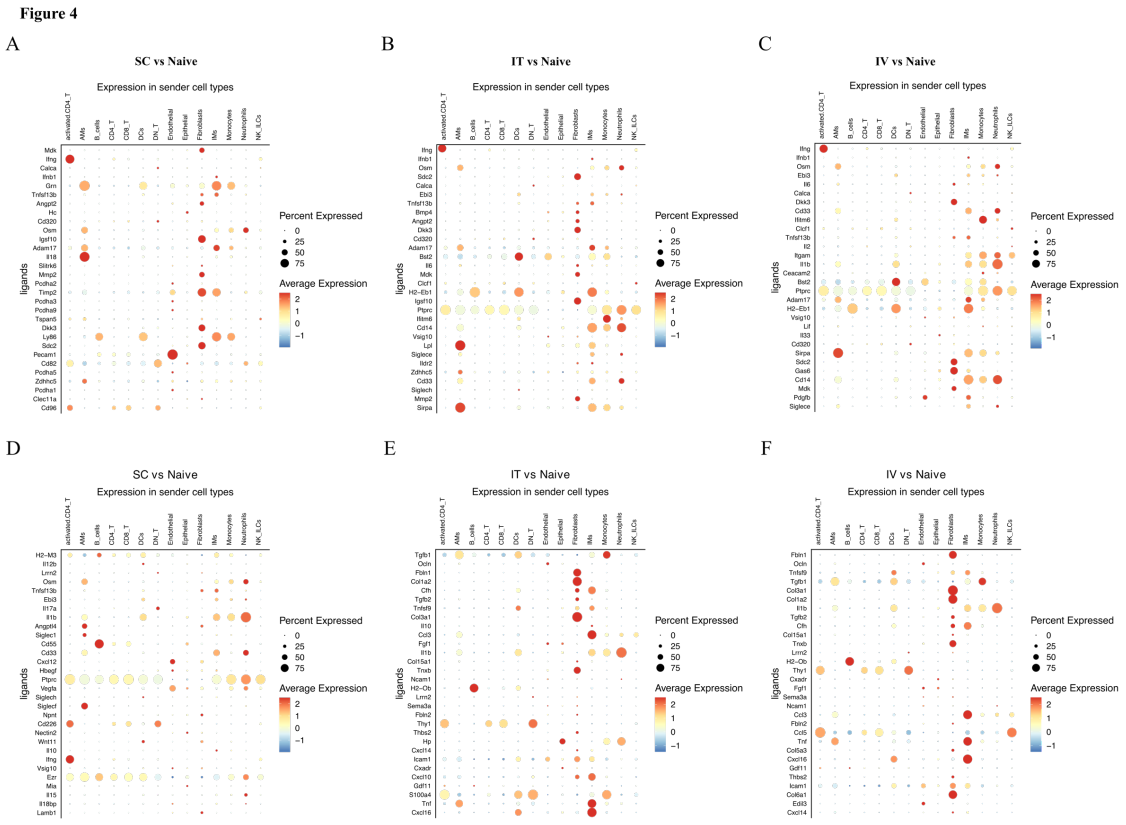

Figure 4. IM-CD4 T cell crosstalk following BCG Vaccination.

(A-C): NicheNet analysis showing the expression of ligands received by IM (compared to Naive) in the sender cell type after each route of vaccination. **(D-F)**: NicheNet analysis showing the expression of ligands received by CD4 T cells (compared to Naive) in the sender cell type after each route of vaccination.

326 **Activated IM localize in distinct tissue niches within the lung.**

327 Since NicheNet had indicated that IM and CD4 T cells may be potential interaction partners, we
328 decided to investigate if these cell types localized to distinct niches within the tissue using spatial
329 transcriptomics. Lung slices were taken 8 weeks after IV, IT or SC BCG, as well as from naïve
330 controls, and analyzed using the 10x Genomics Visium platform. Spatial clustering resulted in 21
331 clusters across the samples (Fig. 5 A, Supplementary Fig. 5 A). Of these, clusters 4, 18 and 19
332 were found predominately in IT and IV slices but not in SC BCG or naïve samples (Fig. 5 B, C,
333 Supplementary Fig. 5 B). To determine the cellular composition of these vaccination induced
334 clusters, we performed cell type deconvolution using RCTD based on our parallel single cell data.
335 This analysis returns weights that estimate the cell type proportions in each spot. Cluster 4 had a
336 bigger proportion of structural cells such as endothelial cells and fibroblasts while cluster 18 and
337 19 were enriched with immune cells. In particular cluster 18 had a higher proportion of IM, B
338 cells, T lymphocytes and other immune cells (Fig. 5 D).

339

340 To assess whether the activated immune cell populations identified in our scRNA-seq analysis
341 localized to IT/IV specific tissue regions we overlaid our activated IM gene expression signature
342 score onto the spatial slices. This signature was highly expressed in the regions occupied by spatial
343 clusters 18 and 19 in the slices taken from IT and IV vaccinated lungs (Fig. 5 E, Supplementary
344 Fig. 5 C). Similarly, B cell and activated CD4 T cell signatures showed strongest expression in
345 these same tissue regions, with the CD4 signature showing somewhat broader distribution across
346 the section (Fig. 5 F, G). Notably, expression of *Cxcl16* and *Cxcr6* was also concentrated in these
347 areas, consistent with our NicheNet predictions of IM-CD4 T cell interactions (Supplementary
348 Fig. 5 F). The co-localization of activated IM, B cells and CD4 T cells suggest that these regions
349 are likely inducible bronchus-associated lymphoid tissue (iBALT), preferentially formed after IT
350 and IV, but not SC, BCG vaccination. Whether proximity to iBALT facilitates rewiring of lung
351 macrophages following BCG vaccination is currently unclear and warrants further investigation.

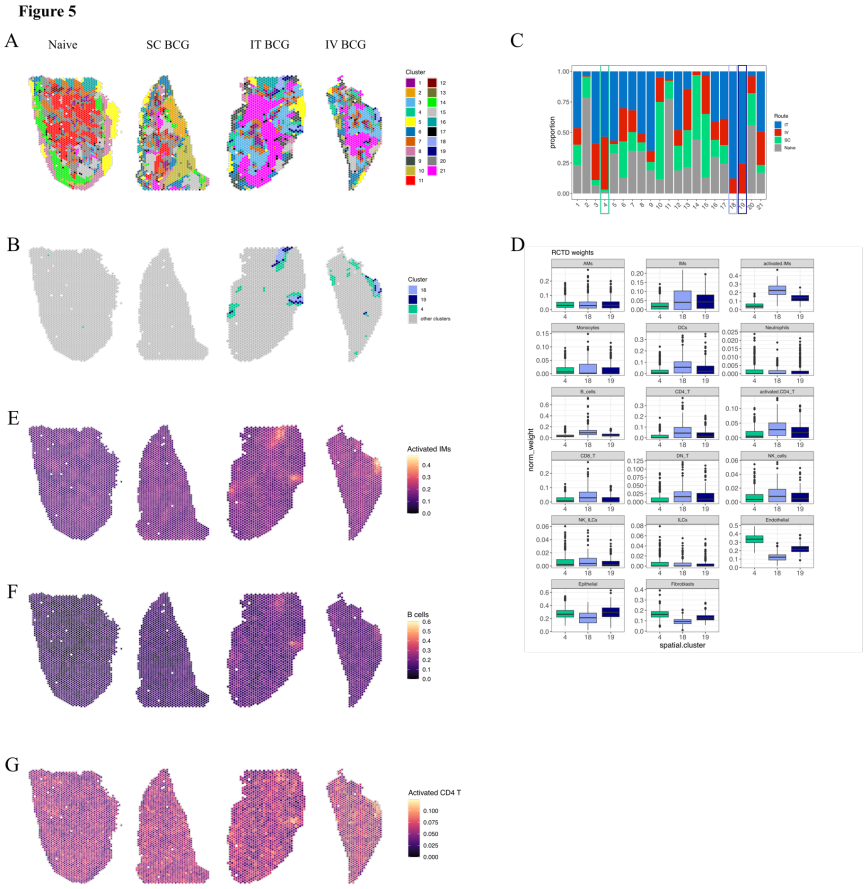

Figure 5. Activated IM localize in distinct tissue niches within the lung.

(A): Spatial images depicting the clusters identified in naïve mice and animals that had been vaccinated 8 weeks previously. **(B):** Spatial images depicting only clusters 4, 18 and 19 in IT and IV BCG vaccinated samples. **(C):** The proportion of each cluster following each route of vaccination as well as in naive conditions. **(D):** RCTD weight plots of the immune and non-immune cells present in cluster 4, 18 and 19. **(E-G)**: Overlay of activated IM (E), B cell (F) and activated CD4 (G) expression signature scores onto spatial slices taken from the lung of mice vaccinated 8 weeks prior as well as from naive animals.

364 **IT BCG vaccination confers superior protection during Mtb challenge.**
365 To assess if the observed changes in IM phenotype and tissue localization following IT BCG
366 translated to superior protection, we performed rechallenge experiments. WT mice were
367 vaccinated with BCG via SC, IV, or IT routes. Sixty days later, vaccinated and unvaccinated mice
368 were challenged with fluorescent Mtb, and lung bacterial burden was measured 14 days post-
369 infection. As compared to unvaccinated controls, mice that had received prior IT vaccination
370 exhibited the greatest reduction in Mtb burden (Fig. 6 A). Flow cytometric analysis confirmed Mtb
371 infection of neutrophils, DCs, AM, and IM, and revealed decreased Mtb signal in these populations
372 in all vaccinated groups (Fig. 6 B and Supplementary Fig. 6 A-D).
373
374 Next, we analyzed the expression of the anti-microbial effector molecule NOS2 across myeloid
375 populations. Among Mtb infected cells, DCs - but not neutrophils - expressed NOS2, and the
376 frequency of NOS2+ DCs increased following SC, but not IT or IV BCG (Fig. 6 F, G,
377 Supplementary Fig. 6 E, F). AM exhibited minimal NOS2 expression in Mtb infected mice and
378 was only slightly enhanced by prior BCG vaccination (Fig. 6 H). Instead, robust NOS2 expression
379 was observed in IM following Mtb infection (Fig. 6 I and supplementary Fig. 6 H). Notably, IM
380 from SC vaccinated mice also expressed significant NOS2 levels after Mtb challenge, despite SC
381 BCG having minimal impact on IM (Fig. 2). Given the higher bacterial burden in SC vaccinated
382 mice, this might reflect infection-driven rather than vaccine-induced NOS2.
383
384 To complement the above data and to more directly assess whether IT BCG enhanced IM effector
385 function in the absence of antigen-specific adaptive immunity, we next established an acute
386 infection model using the opportunistic pathogen *Pseudomonas aeruginosa* (PA). Cohorts of WT
387 mice were vaccinated for 8 weeks as described above and then challenged with PA. 24 hours after
388 infection bacterial burden in the lung was assessed via agar plating. Mice that had received prior
389 IT and IV, but not SC, BCG had significantly reduced bacterial load as compared to unvaccinated
390 mice (Fig. 6J). Using flow cytometry, we observed that the frequency of IM increased after
391 infection and this was most pronounced in mice vaccinated with IT BCG (Fig. 6 K). Additionally,
392 CCR2 expression was increased on IM across all vaccination routes, likely indicative of monocyte
393 influx following PA infection (Fig. 6 L). Within CCR2- IM we observed only minimal NOS2
394 production from unvaccinated mice infected with PA. Instead, these cells expressed Arginase 1

(Arg1), a marker typically associated with the resolution stages of inflammation (Fig. 6 M). PA-induced Arg1 expression may indicate that IM are being skewed away from bacterial control and toward limiting tissue inflammation. Strikingly, prior IT BCG vaccination significantly boosted NOS2 expression by IM while limiting Arg1 (Fig. 6 M, N). Interestingly, we also observed an accumulation of NOS2+Arg1+ double positive IM in IT BCG mice infected with PA (Fig. 6 O). NOS2 and Arg1 expression have traditionally been used as markers of opposing macrophage polarization states, particularly in *in vitro* studies. The presence of an IM population co-expressing both markers suggests macrophage heterogeneity or the concurrent activation of multiple signaling pathways, underscoring the complexity of the inflammatory tissue microenvironment. Collectively our data demonstrate that mucosal BCG administration is protective against both homologous and heterologous bacterial pathogens and point to IM as a central mediator of protection.

Figure 6

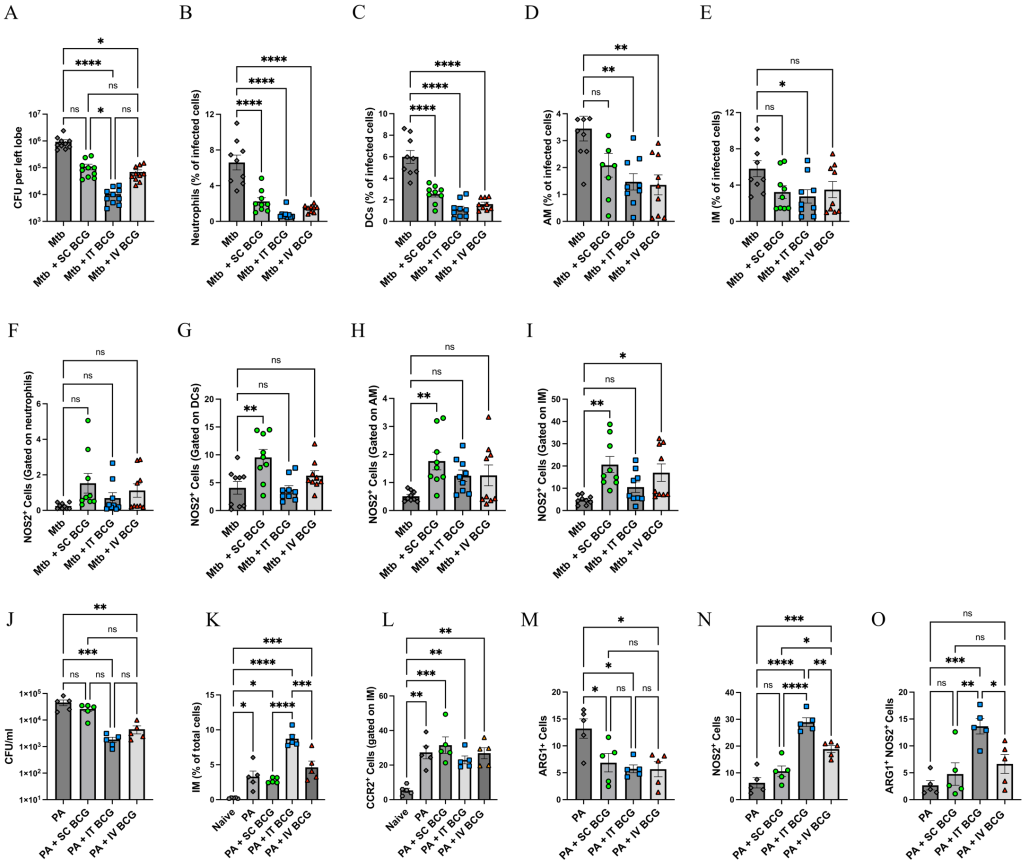

407 **Figure 6. IT BCG vaccination confers superior protection during Mtb challenge.**
408 (**A):** Quantification of Mtb bacterial burden 2 weeks after aerosol infection in unvaccinated mice
409 or in animals that had received SC, IT or IV BCG vaccination 8 weeks previously. **(B-E):**
410 Frequency of infected neutrophils (B), dendritic cells (C), AM (D) and IM (E). **(F-I):** Plots
411 depicting the frequency of NOS2 positive neutrophils (F), DCs (G), AM (H) and IM (I). **(J)**:
412 Quantification of PA burden 24 hours after infection in unvaccinated mice or in animals that had
413 received SC, IT or IV BCG vaccination 8 weeks previously. (K): Frequency of IM following PA
414 infection as in (J). **(L)**: Quantification of CCR2 positive IM following PA infection. **(M-O):**
415 Quantification of Arg1 positive (M), NOS2 positive (N) and double positive IM (O) after PA
416 infection. N: Each datapoint indicates one individual mouse. For A: One-Way ANOVA with non-
417 parametric Kruskal-Wallis Test was performed. For B-O: One-Way ANOVA with Tukey's
418 multiple comparison test was used to determine statistical significance.
419
420 **Discussion.**
421 In this study we investigated how the route of BCG vaccination differentially programs pulmonary
422 macrophages and influences subsequent protection. Using high dimensional flow cytometry, we
423 observed that IT and IV BCG vaccination resulted in similar upregulation of surface and activation
424 markers in AM and IM, while macrophages from SC BCG mice more closely resembled naïve
425 cells. scRNA-seq confirmed that SC BCG induced minimal changes in AM and IM. Notably, our
426 transcriptome data revealed that mucosal IT BCG predominantly rewired lung IM while exerting
427 a less pronounced effect on AM. IM from IT BCG vaccinated mice exhibited enhanced expression
428 of genes downstream of type I/II interferon signaling, as well as metabolic genes involved in
429 glycolysis and oxidative phosphorylation. Our antibiotic data suggest that this IM phenotype is
430 maintained without viable BCG, suggesting potential epigenetic rewiring following vaccination.
431 Future work will incorporate challenge experiments in antibiotic-treated, BCG vaccinated mice to
432 investigate this further.
433
434 Because IM functional capacity may depend on developmental origin, an unresolved question is
435 whether activated IM induced after IT BCG arise from recruited monocytes or from locally rewired
436 resident IM. This could be addressed by flow cytometric analysis of bone marrow to determine
437 whether mucosal BCG alters progenitor composition, combined with genetic fate mapping models

438 to define IM ontogeny. Consistent with systemic progenitor reprogramming, a non-human primate
439 (NHP) study found that mucosal BCG induces transcriptional and metabolic signatures of trained
440 immunity in blood and bone marrow monocytes (23).
441
442 Beyond IM reprogramming, our data further reveal spatially organized IM-CD4 T cell crosstalk
443 as a potential mechanism underlying mucosal vaccine efficiency. Our transcriptome data identified
444 CD4 T cells to be a source of IFNγ, and cell-cell communication analysis suggested reciprocal
445 signaling between IM and CD4 T cells following IT BCG. Mucosal vaccination led to the
446 enrichment of lung-resident CD4 T cells with increased expression of activation markers and
447 chemokine receptors. Spatial transcriptomics further indicated that activated IM localize in close
448 proximity to CD4 T cells within iBALT regions, raising the possibility that IT BCG establishes
449 immune niches that position CD4 T cells and IM for sustained, bidirectional signaling. A previous
450 study demonstrated that a subset of IM is required for iBALT formation in the lung during a house
451 dust mite model (8). However, whether proximity to iBALT is necessary to drive IM activation,
452 particularly during secondary infections, remains unclear. Conceptually, the iBALT niche may
453 facilitate IM-CD4 T cell crosstalk or provide additional cytokine signals beyond IFNγ that
454 influence IM behavior. Experiments that disrupt iBALT formation, e.g. by using LTBR-Fc (27),
455 after BCG vaccination but prior to secondary infection may shed light on this issue.
456
457 These spatial findings raise the possibility that IM guide CD4 T cell localization to and/or within
458 the lung via CXCL16/CXCR6, which in turn facilitates IM activation via T cell derived IFNγ.
459 Supporting this idea, a recent study found CXCL16-positive macrophages situated in close
460 proximity to CXCR6-expressing T cells at the iBALT periphery following influenza infection (24).
461 Future work to assess cytokines in lung homogenates across multiple timepoints post vaccination,
462 as well as the effects of CXCL16 blockade and lymphocyte depletion (25), will help clarify the
463 mechanistic basis of IT BCG induced programming of IM and the requirement for CD4 T cells in
464 this process.
465 In our Mtb challenge model, mice vaccinated with IT BCG demonstrated the strongest protection
466 (i.e. had the lowest bacterial burden) compared to the other routes. This increased protective
467 capacity was not solely attributable to BCG presence in the lung, since IV mice had similar BCG
468 burdens at 4- and 8-weeks post vaccination. We propose that direct IT delivery to the lung

469 facilitates faster uptake of BCG by IM combined with earlier CD4 T cell recruitment, both of
470 which would enable IM epigenetic adaptation. A functional consequence of IM reprogramming is
471 further implied by our *P. aeruginosa* acute infection model, where IM from IT BCG vaccinated
472 mice expressed the highest levels of NOS2. This suggests that IT BCG licenses IM for rapid
473 activation after challenge, thereby facilitating early bacterial clearance. However, while our data
474 strongly implicate IM as key mediators of IT BCG induced protection, we cannot exclude a
475 contributory role for AM, particularly during early pathogen encounter. Future work using recently
476 developed IM-specific (8,9) and AM-specific (26) depletion models will definitively address the
477 relative contributions of each population during bacterial challenge.
478
479 Our findings strengthen the rationale for mucosal BCG as a vaccination strategy and complement
480 recent controlled human infection model studies evaluating the effects of route-specific BCG
481 vaccination in humans (28,29). However, our observation that SC and IV vaccinated mice
482 exhibited similar Mtb burdens appears to diverge from the findings of Darrah et al. (16) who
483 reported superior protection following IV BCG compared to intradermal administration in NHPs.
484 Several factors may contribute to this difference. First, the kinetics and magnitude of BCG induced
485 immunity may differ between mice and NHPs. Second, we assessed Mtb burden at 2 weeks post
486 challenge whereas Darrah et al. evaluated protection at 12 weeks; accordingly, it is possible that
487 IT and IV vaccination would both demonstrate superior protection relative to SC vaccination at
488 later time points in mice. Third, differences in BCG inoculum (1×10^6 in our study versus 5×10^7
489 in Darrah et al.) and/or the dose for Mtb challenge (100-200 CFU in our study versus 4-36 CFU in
490 Darrah et al.) may influence the magnitude of protection.
491
492 In summary, our study demonstrates that the route of BCG vaccination critically shapes pulmonary
493 macrophage reprogramming, with mucosal delivery uniquely licensing IM for enhanced activation
494 potentially through spatially organized immune interactions. These findings establish a
495 mechanistic framework for optimizing mucosal vaccination strategies against tuberculosis and
496 other respiratory pathogens.

497 **Methods**

498 **Key Resource Table**

REAGENT OR RESOURCE	SOURCE	IDENTIFIER
Antibodies		
CD11b BV510 (Clone M1/70)	Biolegend	Cat#101245, RRID:AB_2561390
IA/IE AlexaFluor700 (Clone M5/114.15.2)	Biolegend	Cat#107621, RRID:AB_493726
CD86 PE-Dazzle594 (Clone GL-1)	Biolegend	Cat#105041,RRID:AB_2566408
CD80 BV650 (Clone 16-10A1)	Biolegend	Cat#104731
F4/80 BV605 (Clone BM8)	Biolegend	Cat#123133, RRID: AB_2562305
CCR2 BV421 (Clone SA203G11)	Biolegend	Cat#150605, RRID:AB_2571913
CD64 BV711 (Clone X54-5/7.1)	Biolegend	Cat#139311, RRID:AB_2563846
CD11c BUV395 (Clone HL3)	BD Bioscience	Cat#564080, RRID:AB_2738580.
SiglecF BUV737 (Clone 1RNM44N)	BD Bioscience	Cat# 1RNM44N
CD11a/LFA1 FITC (Clone M17/4)	Biolegend	Cat#101106, RRID: AB_312779
MerTK PE (Clone 2B10C42)	Biolegend	Cat#151505, RRID:AB_2617036
CD45 APC-Fire810 (Clone 30-F11)	Biolegend	Cat103173, RRID:AB_2860599

CD45 Spark NIR 685 (Clone30-F11)	Biolegend	Cat#103168
CD45 Spark Blue 550 (Clone 30-F11)	Biolegend	Cat#103165
CD3 APC (Clone145-2C11)	Biolegend	Cat#100235, RRID:AB_2561455
NKp46 APC (Clone 29A1.4)	Biolegend	Cat#37607, RRID:AB_10612749
CD19 APC (Clone 6D5)	Biolegend	Cat#115512, RRID:AB_313647
iNOS Alexa Fluor 488 (CloneCXNFT)	eBioscience	Cat#53592082
Arg1 eFluor450 (Clone A1EXF5)	eBioscience	Cat#48369780
Lyve1 eFluor450 (Clone ALY7)	eBioscience	Cat#48044380
CD9 PECy7 (Clone MZ3)	Biolegend	Cat#124816
Ly-6G PerCP (Clone 1A8)	Biolegend	Cat#127653
Ly-6C APC Cy7 (Clone HK1.4)	Biolegend	Cat#128025
CD206 Alexa Fluor 647 (Clone C068C2)	Biolegend	Cat#141711
CD169 PerCp Cy5.5 (Clone 3D6.112)	Biolegend	Cat#142409
CX3CR1 BV785 (Clone SA011F11)	Biolegend	Cat#149029
TotalSeq B0301	Biolegend	Cat#155831
TotalSeq B0302	Biolegend	Cat#155833, RRID:AB_2814068
TotalSeq B0303	Biolegend	Cat#155835, RRID:AB_2814069
TotalSeq B0304	Biolegend	Cat#55837, RRID:AB_2814070

TotalSeq B0002 anti-mouse CD8a (Clone 53-6.7)	Biolegend	Cat#100783
TotalSeq B0001 anti-mouse CD4 (Clone RM4-5)	Biolegend	Cat#100573
TotalSeq B0431 anti-mouse CD170 (Clone S17007L)	Biolegend	Cat#155517
TotalSeq B0106 anti-mouse CD11c (Clone N418)	Biolegend	Cat#117359
TotalSeq B0202 anti-mouse CD64 (Clone X54-5/7.1)	Biolegend	Cat#139329
TotalSeq B0813 anti-mouse CD9 (Clone MZ3)	Biolegend	Cat#124823
Bacterial and virus strains		
PAO1 Wild-type *Pseudomonas aeruginosa*	U. Jenal, Biozentrum Basel	ID-UJP505 (28)
PAO1 *CTX::mCherry* chromosomal integration for constitutive expression of mCherry by the pX2 promoter.	U. Jenal, Biozentrum Basel	ID- UJP3715
M. tuberculosis HN878:Turbo635		
M. tuberculosis HN878		
BCG Pasteur	N. Aguiló, University of Zaragoza	N/A
BCG::symc'::mCherry		
BCG:GFP (Pasteur)	N. Aguiló, University of Zaragoza	(18)

Chemicals, peptides, and recombinant proteins		
DAPI	Merk	Cat#D9542-1MG
Liberase TL	Merk	Cat#5401020001
Liberase TM	Merk	Cat#5401119001
DNAse-I	Merk	Cat#10104159001
Collagenase P	Merck	Cat#11213857001
Dispase II	Merck	Cat#D4693
AccuCheck Counting Beads	Invitrogen	Cat#PCB100
Critical commercial assays		
Chromium Next GEM Single Cell 3' Kit v3.1	10x Genomics	Cat#1000269
3' Feature Barcode Kit	10x Genomics	Cat#1000262
Dual Index Kit NT Set A	10x Genomics	Cat#1000242
Chromium Next GEM Chip G Single Cell Kit	10x Genomics	Cat#1000120
Library Construction Kit	10x Genomics	Cat#1000190
Visium Gene Expression Slide and Reagent Kit	10x Genomics	Cat#1000184
Illumina Novaseq 6000	Illumina	Cat#1000724
Deposited data		
Data will be deposited in public repositories.		
Experimental models: Organisms/strains		

Mouse: C57BL/6Rj	Jackson Laboratories	RRID:IMSR_JAX:000664
Software and algorithms		
FlowJo	BD Bioscience	https://www.flowjo.com/solutions/flowjo
GraphPad Prism	GraphPad	https://www.graphpad.com/
Bioconductor R packages (see below)	N/A	https://bioconductor.org/
Gene sets: MsigDB mouse gene sets		https://www.gsea-msigdb.org/gsea/msigdb/index.jsp
Other		
N/A	N/A	N/A

Animals.

C57BL/6Rj (CD45.2) were purchased from Charles River. Mice in each experiment were 6-8 weeks old, same-sex littermates, maintained and bred in the specific pathogen–free animal facility at the University of Basel. All animal experiments were performed in accordance with local and Swiss federal guidelines.

506 **Bacterial culture.**

507 *M. bovis* BCG::symc'::mCherry (hereafter BCG::mCherry) was generated in the laboratory by
508 transformation with the pCHERRY3 plasmid (a kind gift from D. Russell, Cornell University).
509 BCG::mCherry, *M. bovis* BCG Pasteur and BCG:GFP (kindly gifted by N. Aguiló University of
510 Zaragoza) were grown in 7H9 broth (BD) 10% OADC (BD), 0.2% (v/v) glycerol and 0.05% (v/v)
511 Tween 80 (Sigma) under constant shaking at 37° C. After 2 to 4 days the preculture was then
512 diluted 1:100 in 7H9 media without Tween80. When bacteria reached an optical density (OD_{600})
513 of 0.8 to 1, bacteria were collected and washed with PBS (Sigma, D8662). Subsequently bacteria
514 was de-clumped by manual shaking with glass beads and the upper phase containing the single
515 cell suspension was collected. De-clumped bacterial cultures were frozen in 25% glycerol at -80°C
516 until further use. For colony-forming unit (CFU) determination bacterial suspension was plated on
517 7H11 agar plates.

518

519 HN878:turbo635 was generated in house by transformation with the plasmid pCHARGE3 kindly
520 gifted by Tanya Parish (Addgene plasmid # 24658; http://n2t.net/addgene:24658;
521 RRID:Addgene_24658). HN878:turbo635 was grown in 7H9 broth (BD) 10% OADC (BD), 0.2%
522 (v/v) Glycerol, 0.1 mM sodium propionate and 50 mg/ml Hygromycin B (Roth) . Bacteria were
523 de-clumped by vortex shaking with glass beads and the upper phase containing the single cell
524 suspension was harvested and frozen at -80°C until use.

525

526 *P. aeruginosa* (PAO1, PAO1 CTX::mCherry) was kindly provided by U. Jenal, University of
527 Basel. *P. aeruginosa* was cultured in liquid LB and subsequently frozen in 70% glycerol. Prior to
528 infection *P. aeruginosa* was plated from frozen glycerol stock overnight at 37°C on LB agar plates.
529 Single colonies were picked and grown overnight at 37°C under constant shaking (170 rpm).
530 Overnight cultures were then diluted and collected at log phase (OD600 = 0.5).

531

532 ***Mtb* infection.**

533 Prior to aerolization, Mtb was declumped with a 27G metal tip. Mice were infected in an Aero3G
534 Third Generation Aerosolizer (Biaera). Stocks were titrated to result in a day 1 bacterial load of
535 approximately 100 CFU.

536

537 ***BCG / P. aeruginosa* infection.**

538 For intratracheal infections mice were anesthetized with vaporized isoflurane prior to infection
539 than infected intratracheally with $1x10^6$ CFU diluted in 50 µL of PBS (Gibco). For subcutaneous
540 injection $1x10^6$ CFU was delivered 200 µL, while intravenous BCG ($1x10^6$ CFU) was administered
541 in 100 µL PBS.

542

543 **CFU plating.**

544 ***Mtb***: For determination of CFU the left lobe was mechanically homogenized in 1 mL of PBS-
545 Tween (0.05%) using soft tissue homogenizing CK28 prep tubes (Bertin technologies) in a
546 Precellys Evolution Touch homogenizer (Bertin technologies). Homogenates were then serially
547 diluted and plated on 7H11 agar plates containing 10% OADC, 0.2% (v/v) Glycerol, 50 mg/ml
548 Hygromycin B and 1 vial of MGIT PANTA™ Antibiotic mixture (BD). CFU were counted after
549 a 3 week incubation at 37°C.

550 ***P. aeruginosa*:** For determination of CFU lung lobes were digested as described above. 50 uL of
551 digest were removed prior to filtration and a serial dilution was plated on tetracycline selective LB
552 agar plates. CFU were counted after overnight incubation at 37°C.

553

554 **Tissue preparation.**

555 In some experiments, prior to euthanasia mice were anesthetized with vaporized isoflurane and a
556 CD45 (Spark Nir 685) antibody was administered intratracheally. After 20 minutes mice were
557 injected with CD45 (APC-Fire 810) intravenously and sacrificed after 5 minutes.

558 For isolation of macrophages or lymphocytes, lungs were harvested, minced with scissors and
559 digested with a digestion mix containing liberase TM or liberase TL (500 µg/ml, Roche) for 30
560 minutes at 37° C under constant shaking. Single cell suspensions were generated by repeated
561 pipetting and filtering through 70 µm cell strainers (Milteny Biotec) in HBSS buffer (Hanks'
562 Balanced Salt solution, Sigma, H6648-500mL, 0.2% BSA and 0.5 mM EDTA). Erythrocytes were
563 lysed by addition of erythrocyte lysis buffer and the remaining lung cells were washed with HBSS
564 buffer.

565

566

567 **Single cell sequencing.**

568 For isolation of lymphocytes lungs were collected and diced into gentleMACS C Tubes (Miltenyi
569 Biotec) and washed down with 3 ml of media (RPMI, 10 mM aminoguanidine hydrochloride
570 (Sigma-Aldrich), 10 mM Hepes, penicillin-streptomycin-glutamine (100×, Gibco)), prewarmed in
571 a 37° C water bath. Digestion mix containing liberase TL (for lymphoid cells) (33.3 µg/ml, Merk)
572 and deoxyribonuclease I (58 µg/ml; Applichem) was added. Lungs were dissociated on a
573 gentleMACS Dissociator (Miltenyi Biotec) and mashed through 70 µm MACS SmartStrainers
574 (Miltenyi Biotec) as previously described (29). The isolation of stromal cells and myeloid cells
575 lungs has previously been described (30). In short: lobes were minced with scissors and digested
576 with 1mL of RPMI-1640 containing 0.8 mg/ml DispaseII and 0.2 mg/ml Collagenase P (both from
577 Roche), and 0.1 mg/ml DNase I (Invitrogen) at 37° C on a heating block and gently inverted and
578 mixed using a 1mL pipette every 5 min. After 15 min large fragments were spun down (10s) and
579 the supernatant was removed and filtered through a 70 µm MACS SmartStrainer into a tube
580 containing 5mL of Lung Media ((RPMI, 10 mM aminoguanidine hydrochloride (Sigma-Aldrich),
581 10 mM HEPES, penicillin-streptomycin-glutamine (100x, Gibco), 2% FCS, 0.5mM EDTA)).
582 Another 1mL of digestion mix was added to the remaining lung fragments and the process was
583 repeated two more times. Finally, erythrocytes were lysed by addition of ELB (155mM NH4Cl,
584 170mM tris-HCL), remaining cells were washed with FACS buffer (PBS, 2% FCS, and 0.1%
585 sodium azide) and further processed for sorting and subsequent single cell sequencing.

586

587 **Flow cytometry staining.**

588 For all fluorochrome-conjugated antibody dilutions, FACS buffer containing Fc block (Clone
589 2.4G2 InVivoMAb anti-mouse CD16/CD32; BioXCell, #BE0307) was used. Live-dead stain
590 (Zombie Fixable Viability™ Sampler Kit; BioLegend) was added to the antibody mix and stained
591 at RT 10 min. FoxP3 Transcription Factor Staining Buffer Set (eBioscience) was used for
592 intracellular staining. Flow cytometric analysis was performed on Cytek Aurora. Data was
593 analyzed using FlowJo X software (BD) and SpectroFlo (Cytek). Absolute cell numbers were
594 determined using AccuCheck Counting Beads (Invitrogen) based on the manufacturer
595 instructions.

596

597 **Single cell RNA sequencing.**

598 Lungs of naïve or BCG infected mice were removed and processed as described above for isolation
599 of lymphocytes or stromal/myeloid cells. Individual mice were hash tagged using TotalSeq-B anti-
600 mouse hashtag antibodies (B0301-B0304, BioLegend) and TotalSeq-B CITE-seq antibodies
601 (lymphocytes: CD8a (B0002), CD4 (B0001); myeloid cells: SiglecF (B0431), CD11c (B0106),
602 CD64 (B0202), CD9 (B0813)). Live, CD45+ and CD45- cells were sorted from lungs at 80 d.p.i.
603 and submitted for library preparation. A total of 10,000 target cells per sample were loaded. Single-
604 cell capture and cDNA library preparation was performed according to manufacturer's instructions
605 using 10x Genomics Chromium Next GEM Single Cell 3' Kit v2 reagents using dual indexing.
606 Sequencing was carried out on an Illumina Novaseq 6000 at the Genomics Facility Basel, ETH
607 Zurich.
608
609 Raw reads were mapped to the *Mus musculus* reference mm10_ensdb102 using STARsolo (31),
610 and empty droplets were removed with DropletUtils (32,33). The four replicate samples were
611 demultiplexed using hashtag oligos (HTO). Cells were filtered for library size, library complexity,
612 and mitochondrial content using adaptive thresholding implemented in the *perCellQCFilters*
613 function from the R package scuttle with default arguments (34). PCA and UMAP on the PCA-
614 reduced dimensions, were performed using the R package scater (34). Cells were clustered either
615 hierarchically using Ward's method or with the graph-based Leiden method using the bluster R
616 package. Cell annotation was performed with SingleR (35), and pseudo-bulk differential
617 expression analysis was conducted using the *pseudoBulkDGE* function from the scran R package
618 (1.32.0), following the Bioconductor OSCA book
619 (https://bioconductor.org/books/release/OSCA/). Gene set enrichment analysis was performed
620 using camera (36) from the limma R package (37) with MSigDB mouse gene sets. Cell-cell
621 interactions were interrogated using NicheNet (38) following the step-by-step vignette starting
622 from a Seurat object. When possible, lists of differentially expressed genes derived from the
623 pseudo-bulk differential expression analysis were provided to NicheNet for comparison across cell
624 types. Gene signature scores were calculated using UCell (39).
625
626 **Visium Spatial gene expression.**
627 Lungs were inflated with a 1:1 mixture of Tissue-Tek® O.C.T. Compound (Sakura) and PBS and
628 embedded in O.C.T. Tissues were sectioned at 10 µm on a cryostat. Further processing and

placement of sections was performed according to the protocol CG000240 (10X Genomics). Following sample placement, sections were stained with DAPI according to the protocol CG000312 (10X Genomics) and imaged using a Leica DMI 4000/6000 Widefield Microscope. Sections were then permeabilized and prepared for library preparation according to the protocol CG000239 (10X Genomics). Sequencing was carried out on an Illumina Novaseq 6000 at the Genomics Facility Basel, ETH Zurich. The fiducial frame of the Visium slides was aligned using Loupe Browser, and the resulting JSON file was provided to Space Ranger to obtain count matrices. Spots outside the tissue, with library size < 2000, or with mitochondrial content > 10% were filtered out. Spatial clustering was performed using BayesSpace after joining spatial coordinates across samples and integrating transcriptomic data, enabling spatial clusters to be shared between samples (40). The single-cell dataset was used as a reference for deconvolution with RCTD from the spacexr R package (41). Signature scoring and plotting were performed as for single-cell data using Bioconductor 3.19.

Quantification and statistical analysis.

Prism software (GraphPad 10. 4.1) was used for all statistical analyses. Unless otherwise stated One-Way ANOVA with Tukey's multiple comparison test was used to determine statistical significance. Statistical significances are indicated by *p<0.05, **p<0.005, ***p<0.0005, ****p<0.0001, ns, not significant (p > 0.05). In summary graphs, points indicate individual samples. All error bars are mean with SEM.

Acknowledgements.

We are indebted to Gaël Auray and all members of the University of Basel flow cytometry core facilities for cell sorting and troubleshooting, furthermore we thank all staff at the BSL2 and BSL3 animal facilities of the University of Basel. In addition we are grateful to the University of Basel Genomics Core. Bioinformatic calculations were performed at sciCORE (http://scicore.unibas.ch/) scientific computing center at University of Basel. We thank all members of the King laboratory for productive and helpful discussion. This work was supported by the Swiss National Science Foundation, grant 212344 awarded to CGK, the State Secretariat for Education, Research and Innovation (SERI), grant REF-1131.52304 awarded to CGK and the University of Basel Research Fund for Junior Researchers awarded to AJF.

Competing Interests.

All authors declare no conflict of interest in relation to this manuscript.

References.

1. Global tuberculosis report 2025 [Internet]. World Health Organization; Available from: https://www.who.int/teams/global-programme-on-tuberculosis-and-lung-health/tb-reports/global-tuberculosis-report-2025

2. Aegerter H, Lambrecht BN, Jakubzick CV. Biology of lung macrophages in health and disease. Immunity. 2022 Sep;55(9):1564–80.

3. Jeyanathan M, Vaseghi-Shanjani M, Afkhami S, Grondin JA, Kang A, D'Agostino MR, et al. Parenteral BCG vaccine induces lung-resident memory macrophages and trained immunity via the gut–lung axis. Nat Immunol. 2022 Dec;23(12):1687–702.

4. Russell DG, Simwela NV, Mattila JT, Flynn J, Mwandumba HC, Pisu D. How macrophage heterogeneity affects tuberculosis disease and therapy. Nat Rev Immunol. 2025 May;25(5):370–84.

5. Chakarov S, Lim HY, Tan L, Lim SY, See P, Lum J, et al. Two distinct interstitial macrophage populations coexist across tissues in specific subtissular niches. Science. 2019 Mar 15;363(6432):eaau0964.

6. Gibbings SL, Thomas SM, Atif SM, McCubbrey AL, Desch AN, Danhorn T, et al. Three Unique Interstitial Macrophages in the Murine Lung at Steady State. Am J Respir Cell Mol Biol. 2017 Jul;57(1):66–76.

7. Ural BB, Yeung ST, Damani-Yokota P, Devlin JC, De Vries M, Vera-Licona P, et al. Identification of a nerve-associated, lung-resident interstitial macrophage subset with distinct localization and immunoregulatory properties. Sci Immunol. 2020 Mar 13;5(45):eaax8756.

8. Li X, Mara AB, Musial SC, Kolling FW, Gibbings SL, Gerebtsov N, et al. Coordinated chemokine expression defines macrophage subsets across tissues. Nat Immunol. 2024 Jun;25(6):1110–22.

9. Vanneste D, Bai Q, Hasan S, Peng W, Pirottin D, Schyns J, et al. MafB-restricted local monocyte proliferation precedes lung interstitial macrophage differentiation. Nat Immunol. 2023 May;24(5):827–40.

10. Peng W, Vanneste D, Bejarano D, Abinet J, Meunier M, Radermecker C, et al. Endothelial-driven TGFβ signaling supports lung interstitial macrophage development from monocytes. Sci Immunol. 2025;

11. Strickland AB, Chen Y, Sun D, Shi M. Alternatively activated lung alveolar and interstitial macrophages promote fungal growth. iScience. 2023 May;26(5):106717.

12. Dumigan A, Cappa O, Morris B, Sá Pessoa J, Calderon-Gonzalez R, Mills G, et al. *In vivo* single-cell transcriptomics reveal *Klebsiella pneumoniae* skews lung macrophages to promote infection. EMBO Mol Med. 2022 Dec 7;14(12):e16888.

13. Cohen SB, Gern BH, Delahaye JL, Adams KN, Plumlee CR, Winkler JK, et al. Alveolar Macrophages Provide an Early Mycobacterium tuberculosis Niche and Initiate Dissemination. Cell Host Microbe. 2018 Sep;24(3):439-446.e4.

14. Pisu D, Huang L, Narang V, Theriault M, Lê-Bury G, Lee B, et al. Single cell analysis of *M. tuberculosis* phenotype and macrophage lineages in the infected lung. J Exp Med. 2021 Sep 6;218(9):e20210615.

15. Simonson AW, Zeppa JJ, Bucsan AN, Chao MC, Pokkali S, Hopkins F, et al. Intravenous BCG-mediated protection against tuberculosis requires CD4+ T cells and CD8α+ lymphocytes. J Exp Med. 2025 Apr 7;222(4):e20241571.

16. Darrah PA, Zeppa JJ, Maiello P, Hackney JA, Wadsworth MH, Hughes TK, et al. Prevention of tuberculosis in macaques after intravenous BCG immunization. Nature. 2020 Jan 2;577(7788):95–102.

17. Peters JM, Irvine EB, Makatsa MS, Rosenberg JM, Wadsworth MH, Hughes TK, et al. High-dose intravenous BCG vaccination induces enhanced immune signaling in the airways. Sci Adv. 2025 Jan 3;11(1):eadq8229.

18. Mata E, Tarancon R, Guerrero C, Moreo E, Moreau F, Uranga S, et al. Pulmonary BCG induces lung-resident macrophage activation and confers long-term protection against tuberculosis. Sci Immunol. 2021 Sep 24;6(63):eabc2934.

19. Tran KA, Pernet E, Sadeghi M, Downey J, Chronopoulos J, Lapshina E, et al. BCG immunization induces CX3CR1hi effector memory T cells to provide cross-protection via IFN-γ-mediated trained immunity. Nat Immunol. 2024 Mar;25(3):418–31.

20. Pisu D, Johnston L, Mattila JT, Russell DG. The frequency of CD38+ alveolar macrophages correlates with early control of M. tuberculosis in the murine lung. Nat Commun. 2024 Oct 2;15(1):8522.

21. Kohlmeier JE, Cookenham T, Miller SC, Roberts AD, Christensen JP, Thomsen AR, et al. CXCR3 Directs Antigen-Specific Effector CD4+ T Cell Migration to the Lung During Parainfluenza Virus Infection. J Immunol. 2009 Oct 1;183(7):4378–84.

22. Bain CC, MacDonald AS. The impact of the lung environment on macrophage development, activation and function: diversity in the face of adversity. Mucosal Immunol. 2022 Feb;15(2):223–34.

23. Vierboom MPM, Dijkman K, Sombroek CC, Hofman SO, Boot C, Vervenne RAW, et al. Stronger induction of trained immunity by mucosal BCG or MTBVAC vaccination compared to standard intradermal vaccination. Cell Rep Med. 2021 Jan;2(1):100185.

24.de Lima J, Swarnalekha N, Bartoszek E, Litzler LC, Depew CE, Esposito M, et al. HIF-1α+ CD4 T cells coordinate a tissue resident immune cell network in the lung.

25.Kastner AL, Marx AF, Dimitrova M, Abreu-Mota T, Ertuna YI, Bonilla WV, et al. Durable lymphocyte subset elimination upon a single dose of AAV-delivered depletion antibody dissects immune control of chronic viral infection. Immunity. 2025 Feb;58(2):481-498.e10.

26.Verwaerde S, Hastir JF, Schetters STT, Smole U, Seys L, Baptista AP, et al. Innate type 2 lymphocytes trigger an inflammatory switch in alveolar macrophages. Immunity. 2026 Jan;59(1):60-78.e9.

27.Conlon TM, John-Schuster G, Heide D, Pfister D, Lehmann M, Hu Y, et al. Inhibition of LTβR signalling activates WNT-induced regeneration in lung. Nature. 2020 Dec 3;588(7836):151–6.

28.Malone JG, Jaeger T, Spangler C, Ritz D, Spang A, Arrieumerlou C, et al. YfiBNR Mediates Cyclic di-GMP Dependent Small Colony Variant Formation and Persistence in Pseudomonas aeruginosa. Roy CR, editor. PLoS Pathog. 2010 Mar 12;6(3):e1000804.

29.Swarnalekha N, Schreiner D, Litzler LC, Iftikhar S, Kirchmeier D, Künzli M, et al. T resident helper cells promote humoral responses in the lung. Sci Immunol. 2021 Jan 8;6(55):eabb6808.

30.Fletcher AL, Malhotra D, Acton SE, Lukacs-Kornek V, Bellemare-Pelletier A, Curry M, et al. Reproducible Isolation of Lymph Node Stromal Cells Reveals Site-Dependent Differences in Fibroblastic Reticular Cells. Front Immunol [Internet]. 2011 [cited 2026 Jan 30];2. Available from: http://journal.frontiersin.org/article/10.3389/fimmu.2011.00035/abstract

31.Kaminow B, Yunusov D, Dobin A. STARsolo: accurate, fast and versatile mapping/quantification of single-cell and single-nucleus RNA-seq data [Internet]. Bioinformatics; 2021 [cited 2026 Jan 30]. Available from: http://biorxiv.org/lookup/doi/10.1101/2021.05.05.442755

32.participants in the 1st Human Cell Atlas Jamboree, Lun ATL, Riesenfeld S, Andrews T, Dao TP, Gomes T, et al. EmptyDrops: distinguishing cells from empty droplets in droplet-based single-cell RNA sequencing data. Genome Biol. 2019 Dec;20(1):63.

33.Griffiths JA, Richard AC, Bach K, Lun ATL, Marioni JC. Detection and removal of barcode swapping in single-cell RNA-seq data. Nat Commun. 2018 Jul 10;9(1):2667.

34.McCarthy DJ, Campbell KR, Lun ATL, Wills QF. Scater: pre-processing, quality control, normalization and visualization of single-cell RNA-seq data in R. Hofacker I, editor. Bioinformatics. 2017 Apr 15;33(8):1179–86.

35.Aran D, Looney AP, Liu L, Wu E, Fong V, Hsu A, et al. Reference-based analysis of lung single-cell sequencing reveals a transitional profibrotic macrophage. Nat Immunol. 2019 Feb;20(2):163–72.

36.Wu D, Smyth GK. Camera: a competitive gene set test accounting for inter-gene correlation. Nucleic Acids Res. 2012 Sep 1;40(17):e133–e133.

37.Ritchie ME, Phipson B, Wu D, Hu Y, Law CW, Shi W, et al. limma powers differential expression analyses for RNA-sequencing and microarray studies. Nucleic Acids Res. 2015 Apr 20;43(7):e47–e47.

38.Browaeys R, Saelens W, Saeys Y. NicheNet: modeling intercellular communication by linking ligands to target genes. Nat Methods. 2020 Feb 2;17(2):159–62.

39.Andreatta M, Carmona SJ. UCell: Robust and scalable single-cell gene signature scoring. Comput Struct Biotechnol J. 2021;19:3796–8.

40.Zhao E, Stone MR, Ren X, Guenthoer J, Smythe KS, Pulliam T, et al. Spatial transcriptomics at subspot resolution with BayesSpace. Nat Biotechnol. 2021 Nov;39(11):1375–84.

41.Cable DM, Murray E, Zou LS, Goeva A, Macosko EZ, Chen F, et al. Robust decomposition of cell type mixtures in spatial transcriptomics. Nat Biotechnol. 2022 Apr;40(4):517–26.

Figure S1

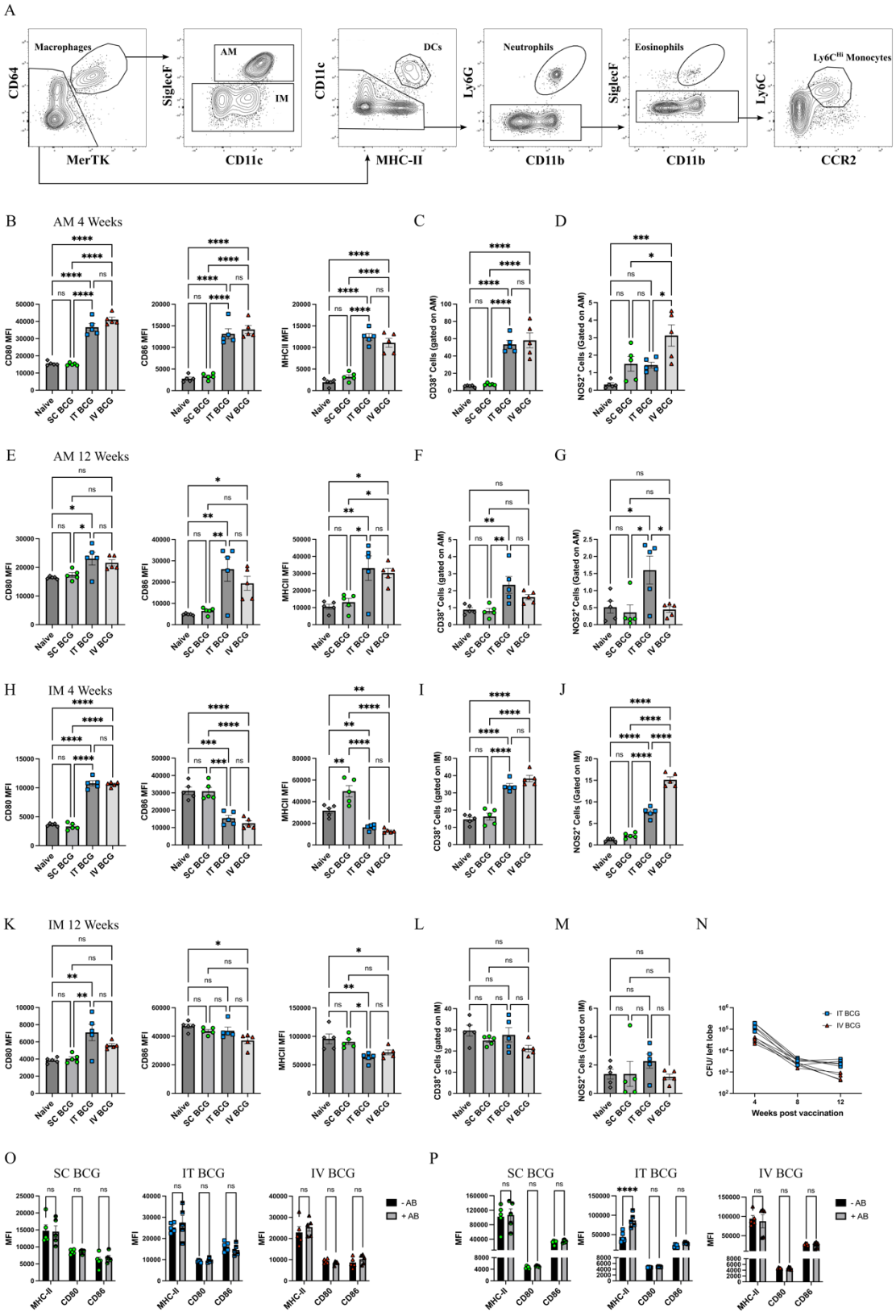
A
Macrophages
CD64
MerTK
SiglecF
AM
IM
CD11c
CD11c
DCs
MHC-II
Ly6G
Neutrophils
CD11b
SiglecF
Eosinophils
CD11b
Ly6C
Ly6C^Hi Monocytes
CCR2
B
AM 4 Weeks
CD80 MFI
CD86 MFI
MHCII MFI
C
CD38⁺ Cells (gated on AM)
D
NOS2⁺ Cells (Gated on AM)
E
AM 12 Weeks
F
G
H
IM 4 Weeks
I
CD38⁺ Cells (gated on IM)
J
NOS2⁺ Cells (Gated on IM)
K
IM 12 Weeks
L
M
N
CFU/ left lobe
Weeks post vaccination
IT BCG
IV BCG
O
SC BCG
IT BCG
IV BCG
MFI
- AB
+ AB
P
Naive
SC BCG
IT BCG
IV BCG
MHC-II
CD80
CD86

800 **Supplementary Figure 1.**

801 **(A)**: Gating strategy used to identify lung innate immune cells including AM, IM, DCs,
802 neutrophils, eosinophils and Ly6C Hi monocytes. Gated on live, CD45+, CD3-, CD19- & Nkp46-
803 cells. **(B)**: MFI of CD80, CD86 and MHCII expression by AM 4 weeks after SC, IT or IV BCG
804 vaccination. **(C, D)**: Frequency of CD38 or NOS2 positive AM from mice vaccinated as in (B).
805 **(E-G)**: MFI of CD80, CD86 and MHCII expression by AM 12 weeks after vaccination (E) and
806 the frequency of CD38 or NOS2 positive cells (F, G). **(H)**: MFI of CD80, CD86 and MHCII
807 expression by IM 4 weeks after SC, IT or IV BCG vaccination. **(I, J):** Frequency of CD38 or
808 NOS2 positive IM from mice vaccinated as in (H). **(K-M)**: MFI of CD80, CD86 and MHCII
809 expression by IM 12 weeks after vaccination (K) and the frequency of CD38 or NOS2 positive
810 cells (L, M). **(N)**: BCG bacterial burden in the lungs of mice vaccinated with IT or IV BCG for 4,
811 8 and 12 weeks. **(O, P)**: MFI of MHCII, CD80 or CD86 expression by AM (O), or by IM (P), in
812 mice that had been vaccinated with BCG and subsequently treated with antibiotics. N: Each
813 datapoint indicates one individual mouse. One-Way ANOVA with Tukey's multiple comparison
814 test was used to determine statistical significance.

815

816

817

818

819

820

821

822

823

824

825

826

827

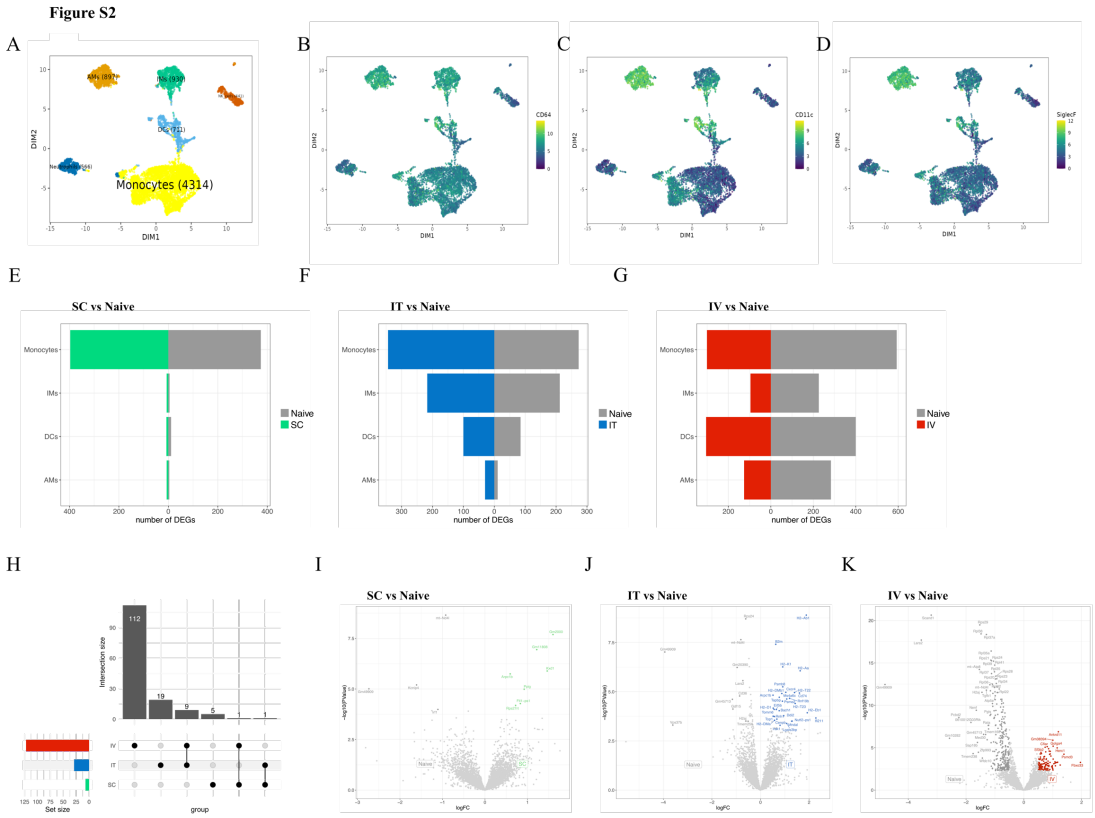

Supplementary Figure 2.

(A): UMAP depicting clusters of AM, IM, DC, neutrophils and DCs identified in single cell RNA Seq dataset. **(B-D):** UMAP depicting protein expression of CD64 (B), CD11c (C) and SiglecF (D). **(E-G)**: Bar plots depicting the number of differentially expressed genes in monocytes, DCs, IM or AM 8 weeks after SC, IT or IV BCG vaccination. **(H)**: Upset plot depicting the number of genes upregulated by AM after each route of BCG vaccination as compared to naïve cells. **(I-K)**: Volcano plots depicting selected genes expressed by AM following SC (I), IT (J) or IV (K) vaccination.

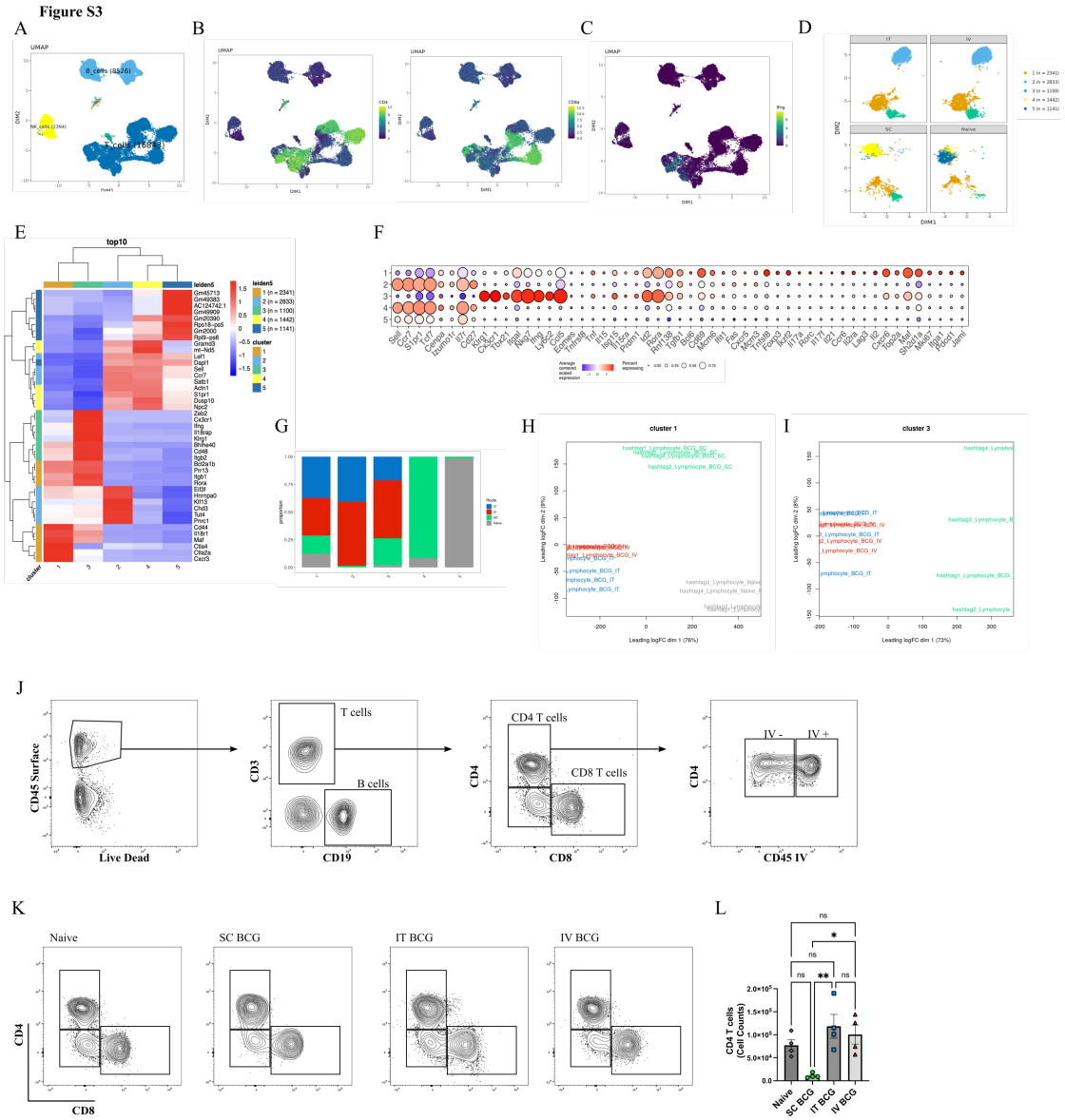

Supplementary Figure 3:

(A, B): UMAP depicting lymphocyte populations identified in scRNA-Seq (A) and protein expression of CD4 and CD8 (B). **(C):** Expression of *Ifng* by the lymphocyte populations identified in (A). **(D)**: Clusters of CD4 T cells identified 8 weeks after SC, IT and IV BCG vaccination. **(E, F)**: Heatmap with the top 10 genes expressed by each cluster of CD4 T cells (E) and the expression of marker genes (F) used to identify the CD4 T cell subsets. **(G)**: Proportion of each cluster of CD4

850 T cells 8 weeks after SC, IT and IV BCG vaccination. **(H, I)**: MDS plots depicting the distribution
851 of cluster 1 and cluster 3 CD4 T cells in each condition. **(J)**: Gating strategy used to identify CD4
852 T cells, gated on live CD45 positive cells. **(K, L)**: Representative plots and cell counts of CD4 T
853 cells in naive and BCG vaccinated mice. For L, N: Each datapoint indicates one individual mouse.
854 One-Way ANOVA with Tukey's multiple comparison test was used to determine statistical
855 significance.
856

Figure S4

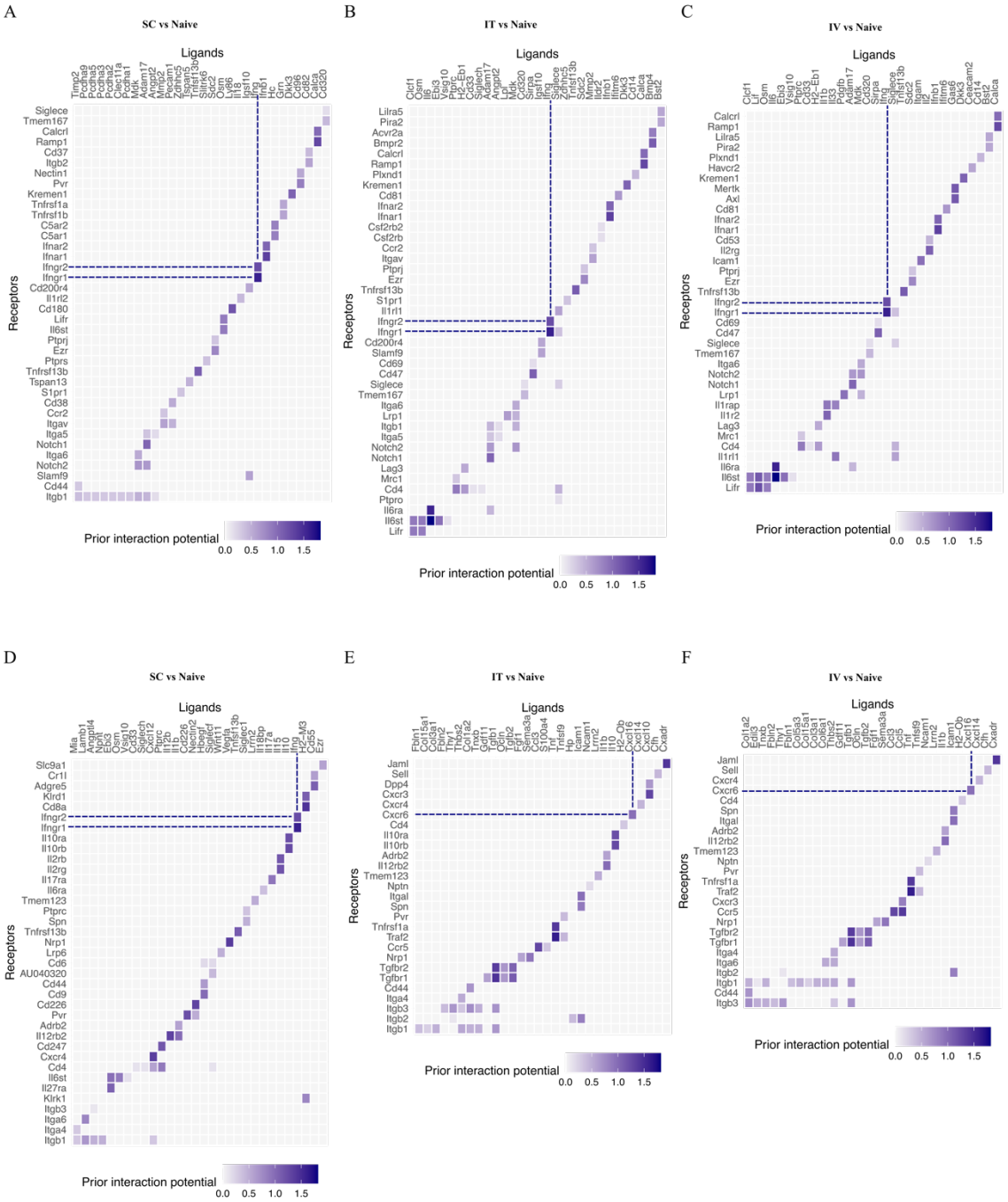
A
SC vs Naive
Ligands
Receptors
Prior interaction potential
0.0 0.5 1.0 1.5
B
IT vs Naive
Ligands
Receptors
Prior interaction potential
0.0 0.5 1.0 1.5
C
IV vs Naive
Ligands
Receptors
Prior interaction potential
0.0 0.5 1.0 1.5
D
SC vs Naive
Ligands
Receptors
Prior interaction potential
0.0 0.5 1.0 1.5
E
IT vs Naive
Ligands
Receptors
Prior interaction potential
0.0 0.5 1.0 1.5
F
IV vs Naive
Ligands
Receptors
Prior interaction potential
0.0 0.5 1.0 1.5

860 **Supplementary Figure 4.**

861 **(A-C):** Heatmap representing NicheNet-predicted interaction potentials for ligand-receptor pairs,
862 between the sender cell types and IM, that are contributing to downstream differentially
863 expressed genes identified comparing BCG SC vs Naïve (A), BCG IT vs Naïve (B) and BCG IV
864 vs Naïve (C). The interaction between *Ifng* and *Ifngr1*/*Ifngr2* is highlighted. **(D-F):** Heatmap
865 representing NicheNet-predicted interaction potentials for ligand-receptor pairs, between the
866 sender cell types and CD4 T cells, that are contributing to downstream differentially expressed
867 genes identified comparing BCG SC vs Naïve (D), BCG IT vs Naïve (E) and BCG IV vs Naïve
868 (F). The interactions between *Ifng* and *Ifngr1*/*Ifngr2* and between *Cxcl16* and *Cxcr6* are
869 highlighted.

870

871

Figure S5

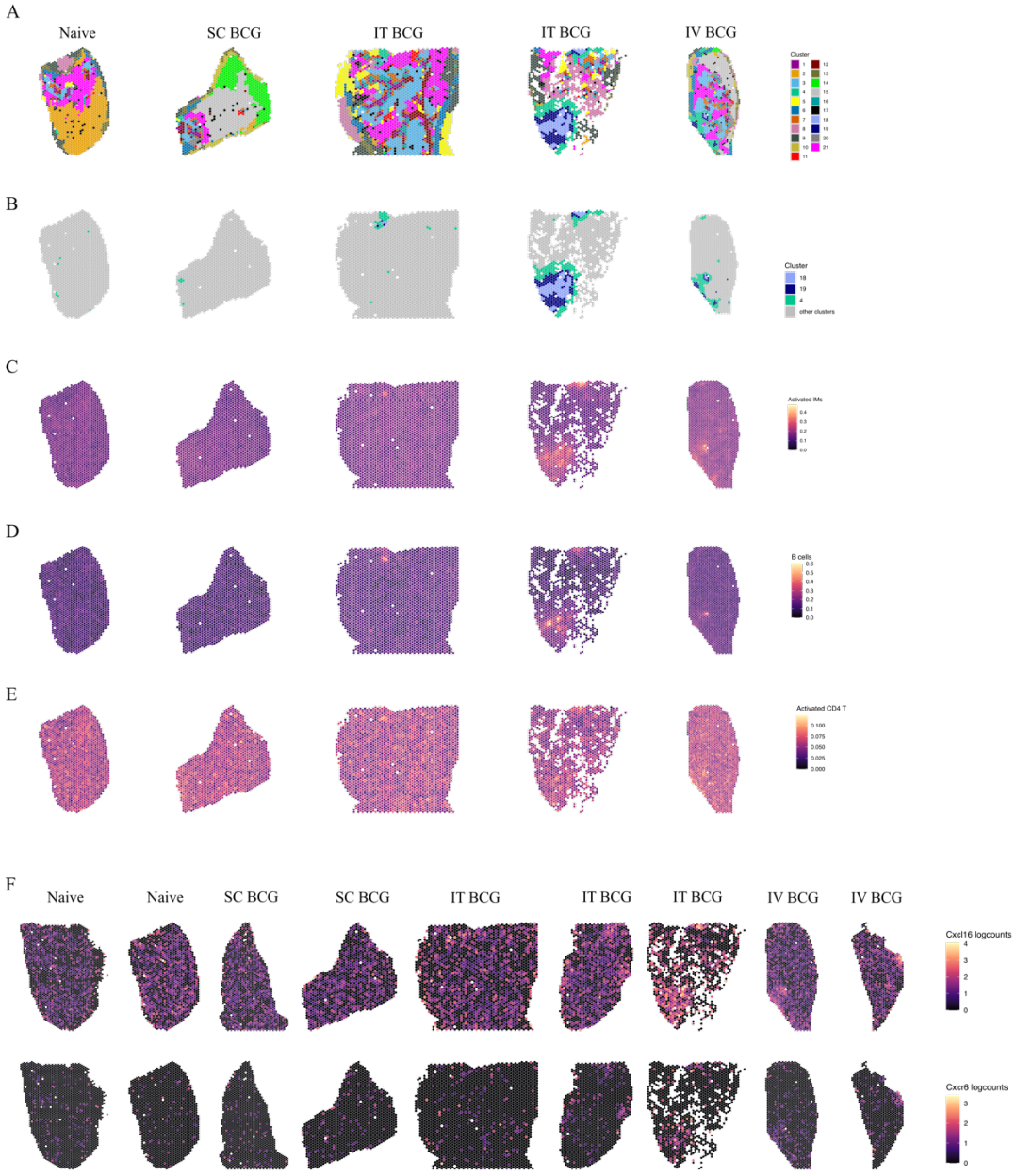
A
Naive
SC BCG
IT BCG
IT BCG
IV BCG
Cluster
B
Cluster
18
19
4
other clusters
C
Activated IMs
D
B cells
E
Activated CD4 T
F
Naive
Naive
SC BCG
SC BCG
IT BCG
IT BCG
IT BCG
IV BCG
IV BCG
Cxcl16 logcounts
Cxcr6 logcounts

Supplementary Figure 5.

(A): Spatial images of additional samples, depicting the clusters identified in naïve mice and animals that had been vaccinated 8 weeks previously. **(B)**: Spatial images of additional samples, depicting only clusters 4, 18 and 19 in IT and IV BCG vaccinated samples. **(C-E):** Overlay of activated IM (C), B cells (D) and activated CD4 T cells (F) expression signature scores onto additional spatial slices taken from the lung of mice vaccinated 8 weeks prior as well as from naive animals. **(F):** *Cxcl16* (top) and *Cxcr6* (bottom) gene expression on all spatial slices taken from the lung of naive animals as well as from mice vaccinated 8 weeks prior.

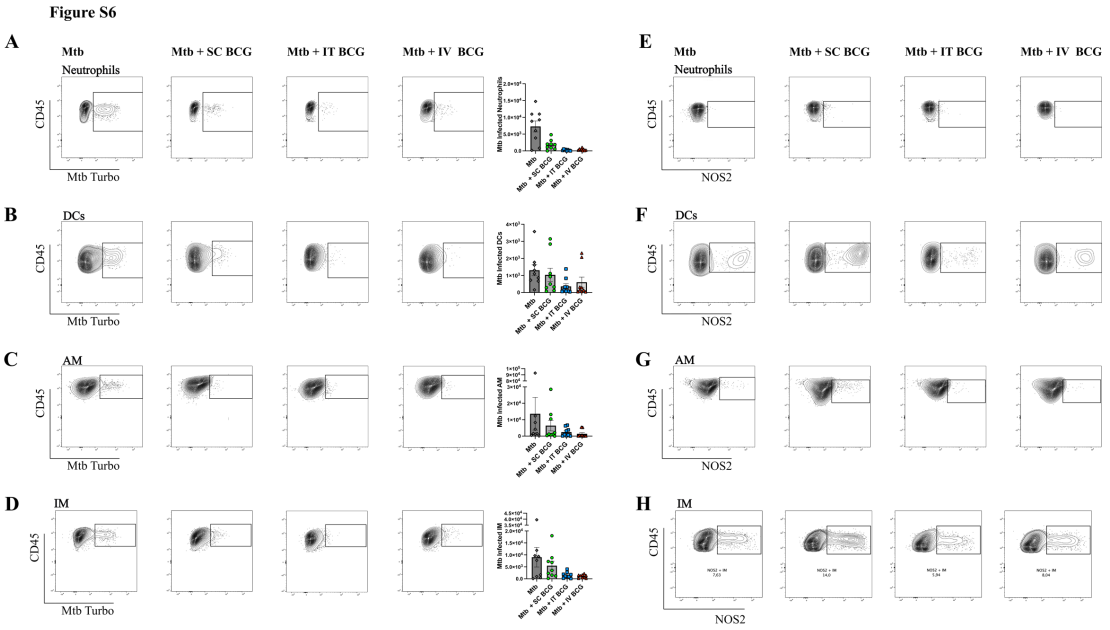

Supplementary Figure 6.

(A-D): Representative FACs plots depicting Mtb infected neutrophils (A), DCs (B), AM (C) and IM (D). Bar plots depict the number of infected cells for each condition. **(E-H)**: Representative FACs plots depicting NOS2 expression in neutrophils (E), DCs (F), AM (G) and IM (H).